Effect of elastic vibrations on normal head-on collisions of isothermal spheres

Ryo Murakami* and Hisao Hayakawa
Yukawa Institute for Theoretical Physics, Kyoto University, Sakyo-ku, Kyoto 606-8502, Japan
(Received 21 September 2013; revised manuscript received 6 December 2013; published 30 January 2014)

We numerically investigate head-on collisions of isothermal viscoelastic spheres. We find that the restitution coefficient oscillates against the impact speed if the solid viscosity inside the sphere is small enough. We confirm that the oscillation arises from the resonance between the duration of contact and the eigenfrequencies of the sphere. This oscillation disappears if there exists the strong solid viscosity in spheres. We also find that a sinusoidal behavior of the restitution coefficient against the initial phase in the eigenmodes for collisions between a thermally activated sphere and a flat wall. As a result, the restitution coefficient can exceed unity if the impact speed of the colliding sphere is nearly equal to or slower than the thermal speed. We have confirmed the existence of the fluctuation theorem for impact processes through our simulation.

DOI: 10.1103/PhysRevE.89.012205 PACS number(s): 45.70.−n, 62.30.+d, 82.60.Qr

I. INTRODUCTION

A granular material is a collection of discrete solid grains characterized by the loss of energy during collisions between grains. Granular materials such as sands and powders are commonly observed not only on Earth [1,2], but also on the other planets and satellites such as Mars [3] and the moon [4] as well as planetary disks [5–9]. Granular material behaves as an unusual liquid or a solid or a gas depending on its setup [10]. It is, of course, important to control the behavior of granular materials in engineering and industry [11–15]. The rich behavior of granular materials mainly arises from inelastic collisions between grains which are the results of competition among attractive, repulsive, and dissipative interactions between contacting grains [2]. Therefore, knowing the properties of the collision processes of grains plays a key role to understanding the physics of granular materials.

Collisions between grains are characterized by the restitution coefficient e, the ratio of the rebound speed to the impact speed, which is usually assumed to be $0 \leqslant e \leqslant 1$. Although the majority of textbooks of elementary mechanics states that e can be treated as a material constant, recent studies on collision dynamics revealed that the restitution coefficient behaves in a more complicated manner: The restitution coefficient depends on the impact speed [16–20], the restitution coefficient can exceed unity in oblique collisions [21–24], and the restitution coefficient can be negative in oblique collisions [25,26]. Recently, Müller *et al*. performed a remarkable experiment and observed the step-wise behavior of the restitution coefficient against the impact speed [27], where a steel sphere of the diameter 6 mm bounces repeatedly off the glass plate. They suggested that the match or mismatch between the vibration frequency of the glass plate and the free flight time is responsible for this stair-wise behavior.

Collisions, however, between small grains such as fine powders, known as cohesive dry powders, are strongly affected by attractive surface force, in particular for slow collisions [11,17,25,28–34]. Note that this attractive force between fine powders is unavoidable because it originates in the interatomic forces such as the van der Waals force. As a result, a variety of processes in collisions of fine powders can be observed depending on their impact speeds [35]. Nanopowders fragment into atoms [36,37] or several large components or bury themselves on walls [38,39] for sufficiently high speed impacts. On the other hand, colliding powders are coalesced if the impact speed is too slow as in adsorptions of powders on walls [40,41] and clustering in freely falling granular streams [42]. It is, however, possible to reduce the attractive force by the surface coating of nanoparticles [43]. Awasthi *et al*. introduced a cohesive parameter which reduces the attractive interaction between atoms on the surface in their numerical model, and simulate the rebound process of a Bi cluster onto a SiO_2 surface [44]. The qualitative validity of such a simplified model has been confirmed by the simulation of an atomicly based model [25].

Needless to say, fine powders have played major roles in recent advanced nanotechnology and nanoscience. Indeed, one of the main purposes of the nanotechnology and nanoscience is to understand, control, and manipulate fine powders. Because these fine powders in nanoscale are intermediate between single small molecules and macroscopic bulk materials, their properties and behavior are qualitatively different from those of their constituent elements and from those of macroscopic pieces of materials. Therefore, it is important to understand the behavior of collisions of fine powders.

It was still believed that the restitution coefficient for normal head-on collisions should be $e \leqslant 1$ because this bound is connected to the second law of thermodynamics. Nevertheless, it is remarkable that this bound is also violated even for normal head-on collisions between nanoclusters, known as "superrebound" for $e > 1$, because thermal fluctuations can play a major role in nanoscale [31,34,45]. Motivated by these findings we only focus on normal head-on collisions, though the tangential force plays important roles in describing the rich behavior of cohesive collisions [46]. In the superrebounds, parts of the elastic vibrations are transferred to the translational motion of the colliding bodies and thus the kinetic energy of the translational motion of it can increase after the collision. The superrebound is associated with the decreases of entropy [34] and the fluctuation theorem [47–54]. Indeed, Tasaki indicated that the probability of the restitution coefficient can satisfy an extended fluctuation theorem if the motion of the center of mass can be separated from the motion of the internal degrees

*ryo-mura@yukawa.kyoto-u.ac.jp

of freedoms [55]. Note that the superrebounds take place only when the impact speed is nearly equal to or slower than the thermal speed, to be consistent with the requirement of the thermodynamics.

The aim of this paper is to clarify the role of collective modes or viscoelastic vibrations inside the grain associated with the energy transfer between the translational motion and the internal modes. For this purpose we extend the method developed for two-dimensional isothermal elastic disks [56,57] to the three-dimensional case. It is remarkable that Aspelmeier performed a three-dimensional simulation by introduction of an exponential potential $e^{-\alpha r}$ with the distance r between atoms on the surface of a colliding sphere in the limit $\alpha \to \infty$. Although his study was a pioneering work using a model of elastic spheres, his model produced some unnatural behavior such as the repeats of discrete contact and free flight during a collision and a harmonic contact force instead of the expected Hertzian force [58]. To improve these points, we propose a new model of colliding isothermal viscoelastic spheres as a natural extension of the previous two-dimensional (2D) models [56,57].

We also consider the effects of the solid viscosity, the attractive interaction on the surface of the colliding spheres or the wall, and the initial temperature. Most of the research on the theory of elasticity assumes that the local deformation takes place without dissipation. However, this treatment is only valid for the infinitesimal motion of local deformation. In real deformation taking place at finite speed the violation of the local force balance takes place at each instance. Thus, there exists a local relaxation process to recover the balance state, which causes the dissipation and the origin of irreversibly. We only consider the dissipation associated with the local motion of atoms as in the usual viscous fluids.

Our method is complementary to the method based on the molecular dynamics simulation [25,28,30,31,33,34], in which we can know the detailed dynamics of the constituent atoms in colliding objects, but it is not appropriate to characterize the macroscopic deformation of the colliding objects. Of course, we cannot address structural phase transitions in the colliding nanoparticles, unlike molecular dynamics simulations [59], but such transitions only take place when the body collides at very high speed. Indeed some studies based on the molecular dynamics simulation [31,33] only observe elastic deformation in the colliding objects for slow impacts. We also stress that the computational cost of our model is essentially independent of the cluster size, in contrast to the molecular dynamics simulation. Nevertheless, our model can consider the relevant effects of surface force which may play a major role in fine powders.

The organization of this paper is as follows. In the next section, we introduce our model of the colliding viscoelastic spheres and explain the setup of our simulation. Section III shows the results of our simulation at $T = 0$, where we investigate the restitution coefficient against the impact speed. It is remarkable that there exists an oscillation of the restitution coefficient against impact speed if the solid viscosity is absent or small, as will be shown in Sec. III A, though such an oscillation disappears for the large solid viscosity as in Sec. III B. We also investigate the excitation of vibrational modes against the contact duration to understand how the restitution coefficient depends on the impact speed. In Sec. III C we verify whether the conventional contact mechanics is reproducible for the low speed collisions between spheres. Section IV exhibits the results of our simulation under the influence of thermal fluctuations. In Sec. IV A we study the mechanism of superrebounds ($e > 1$) for collisions between a thermally activated cluster and a flat wall. We also study the restitution coefficient against the initial phase of the vibration. In Sec. IV B we numerically confirm the fluctuation theorem for inelastic collisions introduced by the author of Ref. [55]. In Sec. IV C we confirm that the collisional heating during a collision is sufficiently small to be consistent with the assumption of our isothermal model. In Sec. V we discuss our results. This section consists of three parts. In Sec. V A we develop the perturbation theory to explain the initial phase dependence of the restitution coefficient. In Sec. V B we investigate the mode transfer when the initial condition contains only one mode excitation to clarify the mechanism of inelastic collisions. In Sec. V C we summarize future work and perspectives. Finally, we summarize our conclusion in Sec. VI. In Appendix A we explain the derivation of the viscoelastic wave equation for isothermal spheres. In Appendix B we summarize the derivation of the stress-free solutions of the wave equation. In Appendix C we explain the role of the fluctuating stress in continuum dynamics and estimate the critical solid viscosity at which the relaxation time originated from the solid viscosity is comparable to the duration of contact. In Appendixes D–F, we summarize the detailed calculations required for our model and results.

II. MODEL

In this section, we introduce our simulation model. As stated in the Introduction, we adopt a model of isothermal viscoelastic spheres. The detailed derivation of the wave equation and its solution under the stress-free boundary condition can be found in Appendixes A and B, respectively, and the textbook by Love [60]. Let us explain a general case in which a viscoelastic sphere is colliding on another viscoelastic sphere, at first. Later, we will restrict our interest to the case of normal head-on collisions between the sphere and a flat wall.

The equations of motion of two colliding viscoelastic spheres $i = 1,2$ for the radius R_i, mass density ρ_i, and mass $M_i \equiv \rho_i 4\pi R_i^3/3$ are given by

$$M_{\rm eff}\ddot{z}_{\rm CM} = -\frac{\partial V(z_{\rm CM},\boldsymbol{u}_1,\boldsymbol{u}_2)}{\partial z_{\rm CM}}, \tag{1}$$

$$\rho_i \frac{\partial^2 \boldsymbol{u}_i}{\partial t^2} = \rho_i \left(1+\gamma_i \frac{\partial}{\partial t}\right)\left\{\left(c_i^{(\ell)}\right)^2 \nabla\nabla\cdot\boldsymbol{u}_i - \left(c_i^{(\rm t)}\right)^2 \nabla\times(\nabla\times\boldsymbol{u}_i)\right\} - \frac{\partial V(z_{\rm CM},\boldsymbol{u}_1,\boldsymbol{u}_2)}{\partial \boldsymbol{u}_i}, \tag{2}$$

where $z_{\rm CM}$ and $\boldsymbol{u}_i$ are, respectively, the distance between the centers of masses of the colliding two spheres and the deformation field. We also introduce the reduced mass $M_{\rm eff} \equiv (1/M_1 + 1/M_2)^{-1}$, the longitudinal and the transverse sound speeds, $c_i^{(\ell)}$ and $c_i^{(\rm t)}$ for the sphere i, and the solid viscosity γ_i. We should note that the viscous terms proportional to γ_i should be associated with the fluctuating stress to satisfy the

fluctuation-dissipation relation or to relax in the equilibrium state (see Appendix C). Nevertheless, such a fluctuating stress is not important in our paper except for the case of large γ_i because the duration time is much shorter than the equilibration time for most of our situations (see Appendix C). Therefore, we simply ignore the random noise terms in this paper. Equation (2) is the viscoelastic wave equation (see Appendix A) for the sphere i, where $V(z_{\rm CM},\boldsymbol{u}_1,\boldsymbol{u}_2)$ is the total interaction potential between atoms on the surface of the projectile and atoms on the surface of the target. Here we assume that the velocity field $\boldsymbol{v}(t;\boldsymbol{x})$ of the elastic sphere is just the time derivative of the displacement $\boldsymbol{v}(t;\boldsymbol{x}) = \partial\boldsymbol{u}(t;\boldsymbol{x})/\partial t$. Within this framework, the longitudinal and transversal solid viscosities are not independent [see Eq. (B17)]. We also assume the isothermal condition for the colliding spheres. In Sec. IV C we check that the assumption is self-consistent.

We assume that Lennard-Jones atoms are distributed on the surface of the colliding sphere with planar density d_i^{-2}, where d_i $(i = 1,2)$ is the diameter of the atoms placed on sphere i. The potential between the surface atoms at distance r is assumed to be described by

$$\phi(r) = 4\epsilon\left[\left(\frac{\sigma}{r}\right)^{12} - g\left(\frac{\sigma}{r}\right)^{6}\right], \tag{3}$$

where ϵ and σ are the depth of the potential well and the diameter of the repulsive core, respectively, and we have introduced the cohesive parameter $0 \leqslant g \leqslant 1$, which reduces the attractive interaction [44]. Although we mainly investigate collisions without the reduction $g = 1$, we also investigate the repulsive collision, $g = 0$ in Secs. III C and V A, and the reduced attractive collision, $g = 0.2$ in Sec IV A. Here, the distance between the atoms on each surface can be written as (see Fig. 1)

$$\begin{aligned} r(\theta_1,\varphi_1;\theta_2,\varphi_2) &= |\boldsymbol{r}(\theta_1,\varphi_1;\theta_2,\varphi_2)| \\ &= |\{\boldsymbol{G}_2 + R_2\boldsymbol{e}_{r2}(\theta_2,\varphi_2) + \boldsymbol{u}_2(R_2,\theta_2,\varphi_2)\} \\ &\quad - \{\boldsymbol{G}_1 + R_1\boldsymbol{e}_{r1}(\theta_1,\varphi_1) + \boldsymbol{u}_1(R_1,\theta_1,\varphi_1)\}|, \end{aligned} \tag{4}$$

where $\boldsymbol{G}_i$ and $\boldsymbol{e}_{ri}$ $(i = 1,2)$ represent the position of the center of mass and the radial unit vector for the sphere i, respectively.

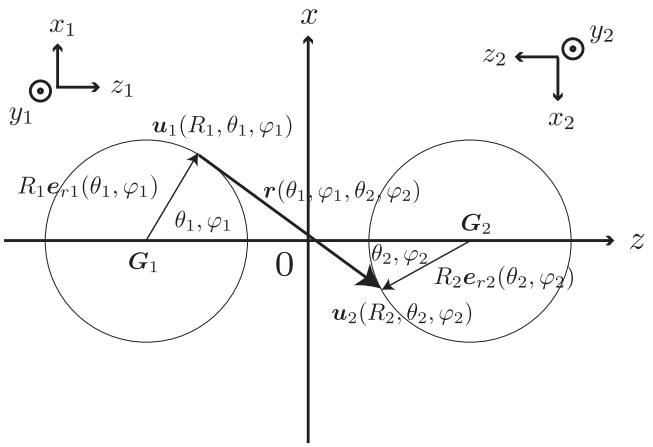

FIG. 1. The coordinate system we adopt, where $\boldsymbol{u}_i(R_i,\theta_i,\varphi_i)$ represents the surface displacement of the cluster i.

Then, the total interaction energy is given by

$$\begin{aligned} &V(z_{\rm CM},\boldsymbol{u}_1,\boldsymbol{u}_2) \\ &= \frac{R_1^2R_2^2}{d_1^2d_2^2}\int_0^{\pi/2} d\theta_1\sin\theta_1\int_0^{2\pi} d\varphi_1\int_0^{\pi/2} d\theta_2\sin\theta_2 \\ &\quad\times\int_0^{2\pi} d\varphi_2\phi[r(\theta_1,\varphi_1;\theta_2,\varphi_2)]. \end{aligned} \tag{5}$$

When vibrational modes are not excited before the collision, the distance $r(\theta_1,\varphi_1;\theta_2,\varphi_2)$ depends only on θ_1,θ_2 and $\varphi_1+\varphi_2$ for head-on collisions. Then, the integration with respect to φ_1 and φ_2 in Eq. (5) can be performed (see Appendix D). On the other hand, when vibrational modes exist before the collision, we cannot execute such an integration even in head-on collisions. If the second sphere (target) is a flat wall, i.e., $R_2 \to \infty$ and the wall is also hard, i.e., $c_2^{(t)}$ and $c_2^{(\ell)}$ are infinite, the displacement of the wall $\boldsymbol{u}_2$ is identical to zero and the potential (5) becomes a simpler form [see Eq. (D6)].

Let us expand $\boldsymbol{u}_i$ in terms of a set of the dimensionless spheroidal modes for the cluster $i = 1,2$ $\tilde{\boldsymbol{u}}^{(\rm S)}_{i,n\ell m}(\boldsymbol{x})$ [see Eq. (B31)]

$$\boldsymbol{u}_i(t;\boldsymbol{x}) = \sum_{n\ell m} Q_{i,n\ell m}(t)\tilde{\boldsymbol{u}}^{(\rm S)}_{i,n\ell m}(\boldsymbol{x}), \tag{6}$$

where n $(n = 0,1,2,\ldots)$, ℓ $(\ell = 0,1,2,\ldots)$, and m $(-\ell \leqslant m \leqslant \ell)$ are the radial, colatitudinal, and azimuthal modes numbers, respectively. We ignore the torsional modes (see Appendix B) because we restrict our interest to normal head-on collisions. Substituting Eq. (6) into Eq. (2), we obtain the equation of motion for the coefficient $Q_{i,n\ell m}(t)$ as follows:

$$\begin{aligned} M_i\ddot{Q}_{i,n\ell m} &= -M_i\omega_{i,n\ell}^2(Q_{i,n\ell m} + \gamma_i\dot{Q}_{i,n\ell m}) \\ &\quad - \frac{\partial V(z_{\rm CM},\{Q_{i',n'\ell'm'}\})}{\partial Q_{i,n\ell m}}, \end{aligned} \tag{7}$$

where $\omega_{i,n\ell}$ is the eigenfrequency of the sphere i (see Appendix B). We numerically solve Eqs. (1) and (7) simultaneously.

For later discussion, let us introduce the eigenenergy $H_{i,n\ell m}(t)$ as follows:

$$H_{i,n\ell m}(t) = \tfrac{1}{2}M_i\{\dot{Q}_{i,n\ell m}(t)\}^2 + \tfrac{1}{2}M_i\omega_{i,n\ell}^2\{Q_{i,n\ell m}(t)\}^2, \tag{8}$$

and the excitation energy $\Delta H_{i,n\ell m}$ as follows:

$$\Delta H_{i,n\ell m} \equiv H_{i,n\ell m}(t_f) - H_{i,n\ell m}(0), \tag{9}$$

where we have introduced the duration time t_f of the collision. Then, the total energy $H_{\rm tot}(t)$ of this system can be written by

$$\begin{aligned} H_{\rm tot}(t) = H_{\rm CM}(t) + \sum_{i,n\ell m} H_{i,n\ell m}(t) + V(z_{\rm CM}(t),\{Q_{1,n'\ell'm'}(t)\}, \\ \{Q_{2,n'\ell'm'}(t)\}), \end{aligned} \tag{10}$$

where $H_{\rm CM}(t)$ is the translational energy of the relative motion

$$H_{\rm CM}(t) = \tfrac{1}{2}M_{\rm eff}\{\dot{z}_{\rm CM}(t)\}^2. \tag{11}$$

In this paper, we mainly investigate collisions between a sphere and a hard wall, and collisions between homogeneous spheres (see Table I). Even when we simulate collisions between two viscoelastic spheres, we assume that the spheres are made of identical atoms. Thus, we can safely remove

TABLE I. The parameter of the object 2 for the collision between the colliding sphere and the flat wall and two spheres.

Sphere and wall	$c_2^{(\mathrm{t})} \to \infty$	$c_2^{(\ell)} \to \infty$	$(R_2 \to \infty)$	
Two spheres	$c_2^{(\mathrm{t})} = c_1^{(\mathrm{t})}$	$c_2^{(\ell)} = c_1^{(\ell)}$	$\rho_2 = \rho_1$	$\gamma_2 = \gamma_1$

TABLE II. The copper's parameters we use in our simulation.

$c^{(\mathrm{t})}$	ρ	Poisson's ratio	ϵ	σ	d
2270 m/s	8960 kg/m^3	0.343	0.415 eV	0.2277 nm	0.256 nm

the subscript of the sphere i for $c^{(\mathrm{t})}$, $c^{(\ell)}$, ρ, and γ for later discussion. To save the computational cost, we truncate the interaction potential at a cutoff distance $z_{\mathrm{cut}} = 5\sigma$, and we place the initial sphere out of the interaction range. We control the incident speed ranging from $0.001c^{(\mathrm{t})}$ to $0.4c^{(\mathrm{t})}$. When we include the effects of the initial thermal fluctuations, we prepare the initial distributions of $Q_{i,n\ell m}(0)$ and $\dot{Q}_{i,n\ell m}(0)$ to satisfy the canonical distributions

$$p_{\mathrm{can}}[Q_{i,n\ell m}(0)] = \sqrt{\frac{M_i\omega_{i,n\ell}^2}{2\pi k_{\mathrm{B}}T}}\exp\left[-\frac{1}{k_{\mathrm{B}}T}\frac{1}{2}M_i\omega_{i,n\ell}^2\{Q_{i,n\ell m}(0)\}^2\right], \quad (12)$$

$$p_{\mathrm{can}}[\dot{Q}_{i,n\ell m}(0)] = \sqrt{\frac{M_i}{2\pi k_{\mathrm{B}}T}}\exp\left[-\frac{1}{k_{\mathrm{B}}T}\frac{1}{2}M_i\{\dot{Q}_{n\ell m}(0)\}^2\right], \quad (13)$$

where we have introduced the temperature T to characterize the variance of the initial fluctuations of modes in Eqs. (12) and (13). When we are interested in collisions not affected by the initial thermal fluctuations, we simply assume that there are no internal vibrations inside the colliding spheres.

We truncate the eigenmodes at the cutoff frequency ω_{cut} due to the limitation of our numerical resources. Thus, the number of radial modes is determined from the condition $\omega_{i,n\ell} < \omega_{\mathrm{cut}}$ for each ℓ, where the number of colatitudinal modes is approximately $\omega_{\mathrm{cut}}R_1/c^{(\mathrm{t})}$. We adopt $\omega_{\mathrm{cut}} = 100c^{(\mathrm{t})}/R_1$ for the axisymmetric case, i.e., $T = 0$, in which the number of colatitudinal modes is 100 and $m \equiv 0$, and we adopt $\omega_{\mathrm{cut}} = 25c^{(\mathrm{t})}/R_1$ for $T \neq 0$, in which the number of colatitudinal modes is 24. The total number of modes is approximately 1500. Figure 2 exhibits the convergence of the restitution coefficient against the cutoff frequency for $T = 0$, $\gamma = 0$. The restitution coefficient begins to converge around $\omega_{\mathrm{cut}} = 25c^{(\mathrm{t})}/R_1$ for both (a) the faster impact $v_{\mathrm{CM}}(0) = 0.1c^{(\mathrm{t})}$ and (b) the slower impact $v_{\mathrm{CM}}(0) = 0.01c^{(\mathrm{t})}$. Thus, the numerical error due to the limitation of the mode number may be sufficiently small for our cutoff frequency.

We adopt the Runge-Kutta-Fehlberg method with adaptive step for the integration of Eqs. (1) and (7). When there is no dissipation, i.e., $\gamma = 0$, the rate of energy conservation, $|H_{\mathrm{tot}}(t) - H_{\mathrm{tot}}(0)|/H_{\mathrm{tot}}(0)$, is kept within 10^{-5}. We adopt the Lebedev quadrature formula, which is the Gaussian quadrature formula for the integration over the surface of a three-dimensional sphere [61] to evaluate the surface integral in Eq. (5) [62]. We adopt the simple trapezoidal rule to evaluate the interactive potential (5) for the axisymmetric case. To avoid unphysical setups, we use some parameters corresponding to the case of the copper for our simulation, which are summarized in Table II [63]. Figure 3 is a series of snapshots of colliding two identical spheres to illustrate its time evolution. The middle figure corresponds to the moment of zero relative speed, where the compression is approximately 20%. In this paper, we mainly investigate collisions for small spheres ($R_1 = 10$ nm), where we will discuss the sphere size dependence of collisions for $T = 0$ in Sec. III A.

III. SIMULATION AT $T = 0$

In this section, we summarize the results of our simulation at $T = 0$. This section consists of three parts. In Sec. III A, we show the results without the solid viscosity $\gamma = 0$. In Sec. III B, we discuss the effects of γ. In Sec. III C, we verify whether the contact mechanics of elasticity is held for slow impacts of elastic spheres.

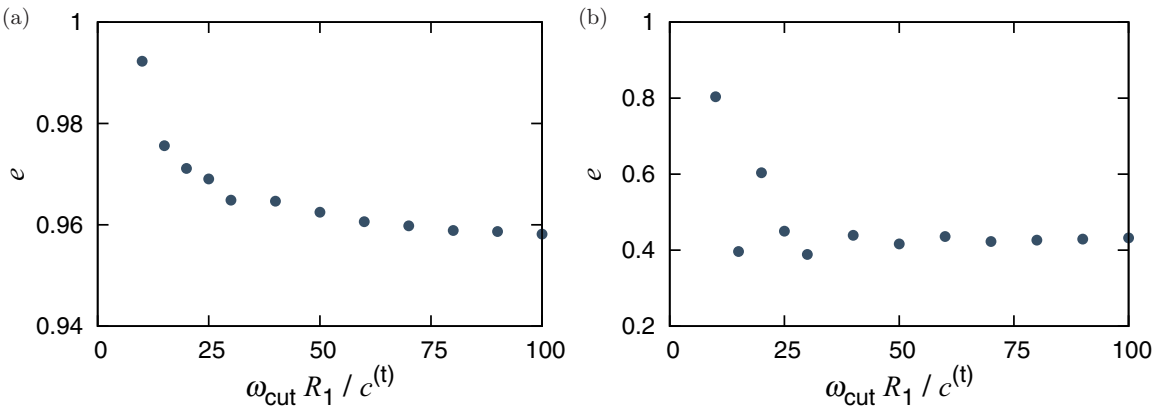

FIG. 2. (Color online) The cutoff frequency ω_{cut} dependence of the restitution coefficient for $T = 0$, $\gamma = 0$, and (a) $v_{\mathrm{CM}}(0) = 0.1c^{(\mathrm{t})}$ and (b) $v_{\mathrm{CM}}(0) = 0.01c^{(\mathrm{t})}$.

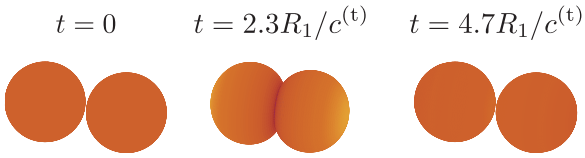

FIG. 3. (Color online) Time evolution of a collision between the identical elastic spheres for $v_{CM}(0) = 0.3c^{(t)}$, $R_2 = R_1$, $T = 0$, and $\gamma = 0$, where the parameters we use are summarized in Table II. The middle figure corresponds to the moment of zero relative speed, in which the compression length of each cluster is approximately 20%.

A. Oscillation of the restitution coefficient for $\gamma = 0$

We here investigate the impact speed dependence of the restitution coefficient for collisions between an elastic sphere ($\gamma = 0$) and a flat wall under an athermal initial condition at $T = 0$, ranging from $v_{CM}(0) = 0.001c^{(t)}$ to $v_{CM}(0) = 0.4c^{(t)}$. Even without dissipation in our model, we can reproduce inelastic collisions characterized by $e < 1$ because the energy is transferred from the translational motion to vibrational modes during the contact. From Fig. 4(a), we find a characteristic oscillation of $e(v_{CM})$. We plot the results for spheres of $R_1 =$ 10 nm, $R_1 = 100$ nm, and $R_1 = 1$ μm in Fig. 4(a). Because we adopt the radius R_1 as the length unit in our simulation, we practically change the parameters proportioned to R_1, such as the core diameter $\sigma = 0.02277R_1$. Here we discuss the size dependence of the collision. The main difference between larger and smaller spheres is the strength of the surface attraction per the volume. Indeed, the "critical speed" below which the colliding spheres are coalesced for the smaller sphere is faster than that for the larger one.

We also investigate the excitation of each mode $\Delta H_{0\ell 0}$ introduced in Eq. (9) against the impact speed, where we only focus on the fundamental modes ($n = 0$) because the excitations of the other modes are much smaller than that of the fundamental modes. Figure 4(b) shows the excitations of the quadrupole ($\ell = 2$) and the octopole ($\ell = 3$) modes against the impact speed. We find the existence of regular oscillatory behavior in these relations.

Then, we replace the impact speed by the contact duration τ, which is only the time scale except for the eigenfrequencies in this system [see Fig. 5(a)]. Here we introduce the potential cutoff V_{cut} to suppress the long-ranged tail effect in the interactions of slow impacts as $V(z_{CM},\{Q_{n\ell 0}\}) = 0$ if the calculated potential is smaller than V_{cut}. Figure 5(a) shows the relation between the excitation $\Delta H_{0\ell 0}$ and the contact duration τ for $V_{cut} = 5 \times 10^{-5} M(c^{(t)})^2$. We find that the oscillation period of $\Delta H_{0\ell 0}(\tau)$ is a constant, where the period for $\ell = 2$ is larger than the period for $\ell = 3$. The oscillatory behavior is supposed to be caused by the resonance between the duration of contact and the oscillation period of vibration of each mode. To confirm this conjecture, we evaluate the arithmetic mean of the intervals $\langle \Delta\tau_{0\ell}\rangle_{ar}$ between the local minimums of $\Delta H_{0\ell 0}(\tau)$, and compare it to $2\pi/\omega_{0\ell}$ for all the fundamental modes as plotted in Fig. 5(b). They are in good agreement with each other except for cases with very large $\ell(\geqslant 30)$, and thus we can conclude that oscillations of $e(v_{CM})$ and $\Delta H_{0\ell 0}(v_{CM})$ are caused by the resonance between the duration of contact and the vibration period of each mode. The difference between $\langle \Delta\tau_{0\ell}\rangle_{ar}$ and $2\pi/\omega_{0\ell}$ for larger ℓ may originate from the limitation of the resolution of the duration, which is approximately $0.1R_1/c^{(t)}$ [see Fig. 5(a)].

B. Restitution coefficient for finite solid viscosity

In this section, we study collisions of viscoelastic spheres for finite γ at $T = 0$. Figure 6 exhibits the results of $e(v_{CM})$ for finite γ, where the oscillation of $e(v_{CM})$ still remains for $\gamma = 0.01R_1/c^{(t)}$, whereas it disappears for $\gamma = 0.1R_1/c^{(t)}$. It should be noted that the behavior of the restitution coefficient for small γ is quite different from the known results from the quasistatic theory, but its behavior for $\gamma = 0.1R_1/c^{(t)}$ is similar to the known one. Indeed, the solid line in Fig. 6(b) represents the theoretical prediction of cohesive collisions between viscoelastic spheres [29], where the force between cohesive spheres is described as the function of the contact radius a and the speed $\dot{a}$ as

$$F(a,\dot{a}) = \frac{4Y_{eff}a^3}{3R_{eff}} - \sqrt{8\pi Y_{eff}G}a^{3/2} + \gamma\dot{a}\frac{\partial}{\partial a}F(a,\dot{a}), \quad (14)$$

where

$$R_{eff} \equiv \left(\frac{1}{R_1} + \frac{1}{R_2}\right)^{-1}, \quad (15)$$

$$Y_{eff} \equiv \left(\frac{1-\nu_1^2}{Y_1} + \frac{1-\nu_2^2}{Y_2}\right)^{-1}, \quad (16)$$

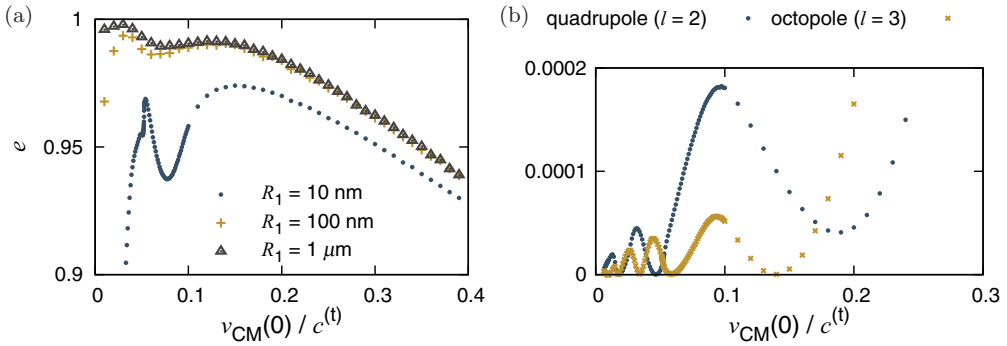

FIG. 4. (Color online) (a) The restitution coefficient as a function of the impact speed without dissipation $\gamma = 0$ and (b) the excitation of the quadrupole ($\ell = 2$) and the octopole ($\ell = 3$) modes as a function of the impact speed.

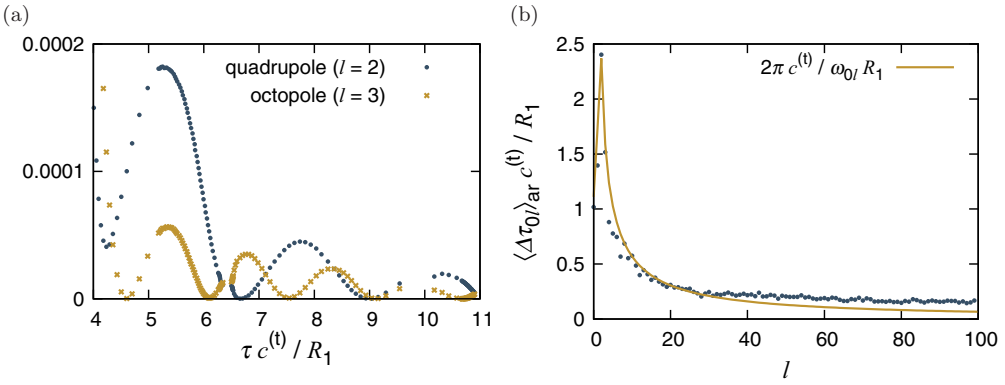

FIG. 5. (Color online) (a) The excitation of the quadrupole and the octopole modes against the contact duration and (b) the arithmetic mean of the intervals $\langle \Delta\tau_{0\ell}\rangle_{\rm ar}$ between the local minimums of $\Delta H_{0l0}(\tau)$ for all the fundamental modes. The solid line in (b) represents the inverse of eigenfrequencies $2\pi/\omega_{0\ell}$.

are, respectively, the reduced radius and effective Young's modulus of two spheres with Young moduli Y_1, Y_2 and Poisson's ratios ν_1, ν_2. G in Eq. (14) is the surface tension satisfying $G = 25\pi\epsilon\sigma^4/24d^6$ [31,64]. We note that the coefficient γ in the third term on the right-hand side of Eq. (14) is identical to that used by Brilliantov *et al.* [29] if there exists only one solid viscosity γ for collisions between spheres of identical constituents (see Appendix E). We numerically solve the equation of motion with the force (14) using the fourth-order Runge-Kutta method with adaptive time interval and plot the solid line in Fig. 6(b) without any fitting parameter. It is easily verified that the theory reproduces the qualitative behavior of the restitution coefficient, but there is no quantitative agreement with the simulation for $\gamma = 0.1R_1/c^{(t)}$. So far we do not identify the reason why we have large dissipation in the simulation. One of the possibilities is that the model we use, Eq. (2), may not correspond to the quasistatic model. Indeed, there is a vibrational excitation in our model in addition to the solid viscosity for the dissipation mechanism. Another possibility is that the deviation may come from the neglect of the fluctuating stress at the finite temperature introduced in Appendix C. As mentioned in the Appendix, the fluctuating stress may play a role for large γ, but we simply ignore its role.

C. Contact mechanics

In this section we investigate the deformation of elastic spheres under an applied force $F_z \equiv -\partial V/\partial z_{\rm CM}$ during slow impacts, $v_{\rm CM}(0) = 0.01c^{(t)}$, at the pole $(r,\theta,\phi) = (R_1,0,0)$ ($\gamma = 0$). First we study the case that the attractive force between the spheres exists. The solid line in Fig. 7(a) represents the prediction of Johnson-Kendall-Roberts (JKR) theory [17,65]. Here, the force F_z in the vertical line is scaled by the reduced radius $R_{\rm eff}$ and Young's modulus $Y_{\rm eff}$. When we simulate collisions between an isothermal elastic sphere and the wall with the cohesive parameter $g = 1$, we found an interesting hysteresis loop in the contact force as reported by Tanaka *et al.* [33]. The time evolution of the contact force is almost reproducible by the JKR theory [17,65], though the theory cannot reproduce the hysteresis loop as reported in a molecular dynamics (MD) simulation [33]. In summary, we verify the relevancy of the theory of elasticity even for the quasistatic contact process.

Next we study the repulsive case for $g = 0$ [Fig. 7(b)]. So far we have mainly simulated collisions between an isothermal elastic sphere and a flat wall. We also simulate collisions between two isothermal elastic spheres with different radii and identical Young's moduli and Poisson's ratios to verify the validity of the theory of elasticity in the quasistatic region

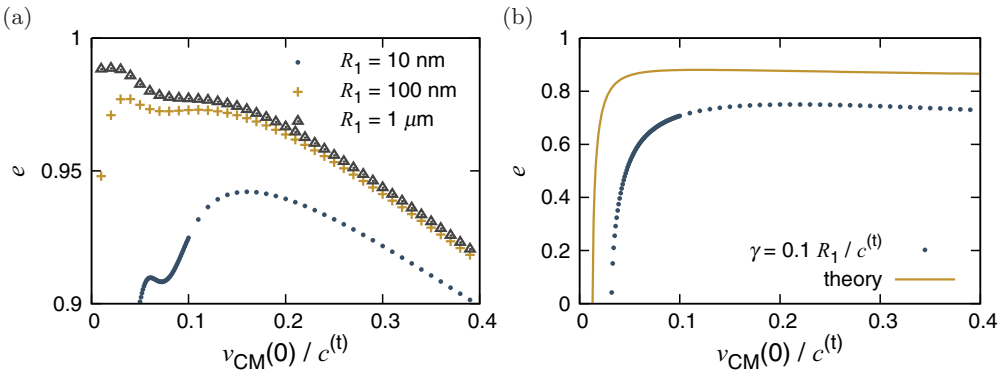

FIG. 6. (Color online) The restitution coefficient against the impact speed for (a) $\gamma = 0.01R_1/c^{(t)}$ and (b) $\gamma = 0.1R_1/c^{(t)}$, respectively. The solid line in (b) represents the theoretical prediction of cohesive collisions between viscoelastic spheres.

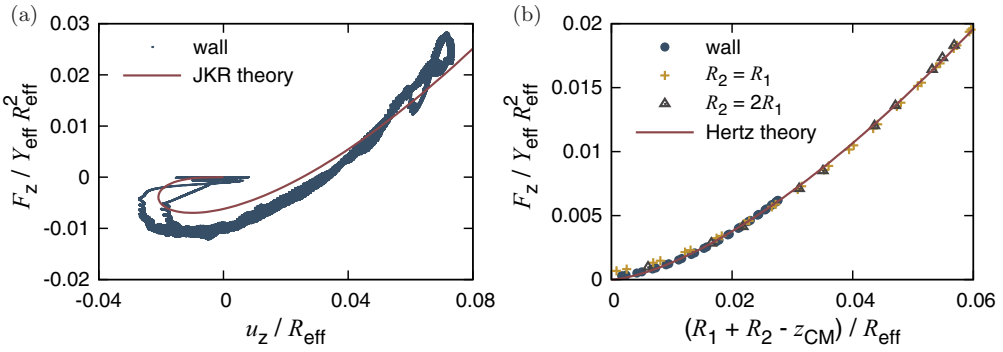

FIG. 7. (Color online) The scaled force as a function of the displacement at the pole $(r,\theta,\phi) = (R_1,0,0)$ without the solid viscosity for (a) the attractive ($g = 1$) and (b) the repulsive ($g = 0$) cases, respectively. Here, "wall" represents the results of simulation for collision between the sphere and the wall.

[66,67]. Figure 7(b) plots the scaled force $F_z/Y_{\rm eff}\sqrt{R_{\rm eff}}$ for collisions between an elastic sphere with the radius R_1 and the wall ($R_2 \to \infty$), between an identical sphere with $R_2 = R_1$, and between a sphere with R_1 and a sphere with $R_2 = 2R_1$ for $v_{\rm CM}(0) = 0.01c^{(t)}$. Here we plot $R_1 + R_2 - z_{\rm CM}$ ($R_1 - z_{\rm CM}$ for the collision with the wall) as the horizontal coordinate, while we plot the displacement $u_z(R_1,0,0)$ for the attractive case. As expected from the theory of elasticity, we verify that the scaled force $F_z/Y_{\rm eff}\sqrt{R_{\rm eff}}$ for the three-dimensional simulation can reproduce the contact theory which is independent of the target radius R_2. Though the value of the horizontal coordinate needs a shift of the origin because we use the soft potential, where the solid line in Fig. 7(b) predicted by the Hertz theory [67] is perfectly on the simulation data only shift of the origin in the horizontal coordinate.

IV. COLLISION AT FINITE T

In this section, we study collisions under the influence of thermal fluctuations ($T \neq 0$). Here we restrict our interest to collisions of the small sphere ($R_1 = 10$ nm), which is strongly fluctuated at finite temperature against the wall. This section consists of three parts. In Sec. IV A, we discuss the mechanism of superrebounds $e > 1$ in detail. In Sec. IV B, we verify the existence of the extended fluctuation theorem proposed by Tasaki [55]. In Sec. IV C, we confirm the theoretical consistency in which the heating induced by collisions is sufficiently small to be consistent with the isothermal elastic model.

A. Superrebounds

In this section, we study the mechanism of super rebounds where the restitution coefficient exceeds unity. We take 1000 samples for each impact in Fig. 8 at $T = 2.14 \times 10^{-8} M(c^{(t)})^2$ (300 K in the physical unit). We only observe either conventional inelastic collisions, i.e., $e < 1$ or coalescence for $g = 1$, whereas we observe superrebounds $e > 1$ for the suppressed attraction case $g = 0.2$.

We investigate the emergence probability of three modes in the collisions: (i) bouncing, (ii) normal inelastic collision for $e < 1$, and (iii) superrebounds for $e > 1$. Figure 9 shows the phase diagram which is obtained under the fixed cohesive parameter $g = 0.2$, where P represents the probability to observe each mode. We take 1000 samples to evaluate P. This phase diagram exhibits that the regions for the bouncing (i) decrease with the increase of the impact speed. The superrebounds can be observed within the range of impact speed $v_{\rm CM}(0) \leqslant 0.013c^{(t)}$. In addition, the probability to appear in the superrebounds has a peak at $v_{\rm CM}(0) = 0.009c^{(t)}$ due to the resonance with eigenmodes.

Figure 10 shows the relation between the restitution coefficient and the solid viscosity γ for the impact speed $v_{\rm CM}(0) = 0.009c^{(t)}$. We find that the events of superrebounds decrease as γ increases, and disappears for $\gamma > 6 \times 10^{-4} R_1/c^{(t)}$.

Here we focus on samples for $v_{\rm CM}(0) = 0.007c^{(t)}$, in which the probability of superrebounds becomes the local minimum against the impact speed (see Fig. 9), and samples for $v_{\rm CM}(0) = 0.009c^{(t)}$ to clarify the mechanism of superrebounds.

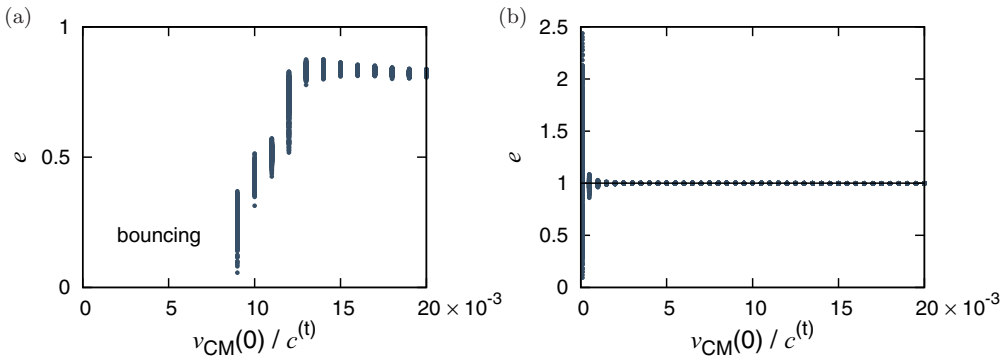

FIG. 8. (Color online) The impact speed dependence of the restitution coefficient for $T = 2.14 \times 10^{-8} M(c^{(t)})^2$ case with fixing (a) $g = 1$ and (b) $g = 0.2$, respectively. The temperature corresponds to 300 K in the physical unit.

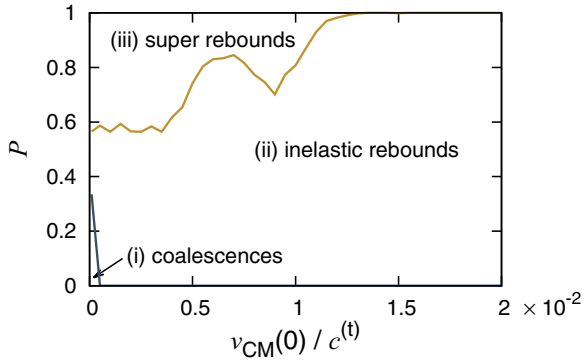

FIG. 9. (Color online) Probability diagrams classified by the three collision modes for $g = 0.2$. The regions (i), (ii), and (iii) represent coalescences, ordinary inelastic rebounds, and superrebounds, respectively.

In Figs. 11(a)–11(c) correspond to the results for $v_{CM}(0) = 0.007c^{(t)}$, while Figs. 11(a′), 11(b′), and 11(c′) correspond to the results for $v_{CM}(0) = 0.009c^{(t)}$. Figures 11(a), 11(a′), 11(b), and 11(b′) exhibit the relations between the restitution coefficient and the initial phase of either the quadrupole ($\ell = 2$) mode or the 16-pole ($\ell = 4$) mode. Here the initial phase $\alpha_{n\ell m}$ is determined by

$$Q_{n\ell m}(0) = \frac{1}{\omega_{n\ell}}\sqrt{\frac{2H_{n\ell m}(0)}{M}}\sin\alpha_{n\ell m}(0). \tag{17}$$

We find the sinusoidal structure of the restitution coefficient in Figs. 11(a), 11(a′), and 11(b′), whereas Fig. 11(b) displays the uniform distribution. In particular, the curve for $v_{CM}(0) = 0.007c^{(t)}$ and $\ell = 2$ [Fig. 11(a)] has a very large amplitude. These results suggest that the initial phases for some modes play key roles in generating superrebounds. We also investigate the excitation energy of each mode with the collision. Figures 11(c) and 11(c′) show the averaged excitation energy $\langle\Delta H_{0\ell 0}\rangle$ of the fundamental ($n = 0$) and the axial ($m = 0$) modes scaled by the initial kinetic energy $H_{CM}(0) = M\{v_{CM}(0)\}^2/2$, where the error bar in these figures represents the standard deviation. The quadruple ($\ell = 2$) mode is strongly excited for $v_{CM}(0) = 0.007c^{(t)}$, whereas its excitation is suppressed and the 16-pole ($\ell = 4$) mode is most excited for $v_{CM}(0) = 0.009c^{(t)}$. The excitation energy seems to be correlated with the amplitude of the sinusoidal curve.

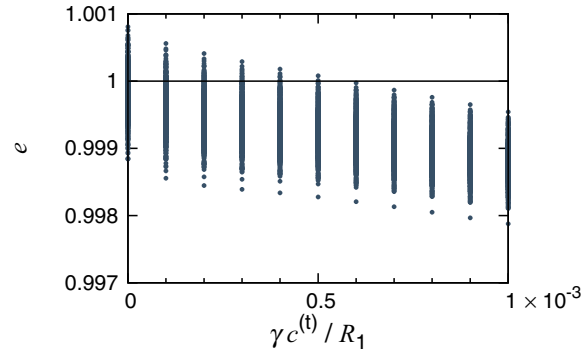

FIG. 10. (Color online) The restitution coefficient against the solid viscosity γ for the impact speed $v_{CM}(0) = 0.009c^{(t)}$.

Indeed, we will examine the perturbation theory of Eqs. (1) and (7) to clarify the mutual relationship in Sec. V A. It should be noted that the excitation of the quadrupole mode for $v_{CM}(0) = 0.009c^{(t)}$ is approximately 20 times smaller than the excitation for $v_{CM}(0) = 0.007c^{(t)}$ in spite of the faster collision. The quadrupole mode is the lowest-order mode. Thus, the quadrupole may be most strongly excited unless the resonance between the collision and the oscillation takes place. The large suppression of the quadrupole excitation may also cause the probability of superrebounds to be large at $v_{CM}(0) = 0.009c^{(t)}$.

B. Fluctuation theorem

Fluctuation theorem states that the ratio of the probability of positive entropy production to the probability of negative entropy production can be expressed by an exponential function in systems out of equilibrium [47,68]. Under an assumption of separation between the macroscopic translational mode and the microscopic internal modes, Tasaki extended the fluctuation theorem to the case of inelastic collisions [55]

$$\frac{P(X_0 \to X_1)}{P(\overline{X}_1 \to \overline{X}_0)} = e^{-W(X_0\to X_1)/k_B T}, \tag{18}$$

where $X_0 \equiv [z_{CM}(0), v_{CM}(0)]$ and $X_1 \equiv [z_{CM}(t_f), v_{CM}(t_f)]$ are the macroscopic variables at the initial and final states, respectively, while $\overline{X}_0 = [z_{CM}(0), -v_{CM}(0)]$ and $\overline{X}_1 = [z_{CM}(t_f), -v_{CM}(t_f)]$ are the states obtained by reversing all the velocity in X_0 and X_1, respectively. Here, $P(X_0 \to X_1)dX_1$ is the transition probability of the macroscopic states from fixed X_0 into the interval between X_1 and $X_1 + dX_1$ and $P(\overline{X}_1 \to \overline{X}_0)d\overline{X}_0$ is the transition probability from fixed $\overline{X}_1$ into the interval between $\overline{X}_0$ and $\overline{X}_0 + d\overline{X}_0$, and $W(X_0 \to X_1) \equiv M[\{v_{CM}(t_f)\}^2 - \{v_{CM}(0)\}^2]/2$ is the macroscopic energy loss during the transition from X_0 to X_1. If $W(X_0 \to X_1) > 0$, $P(X_0 \to X_1)dX_1$ is the probability of superrebounds, which is an exponentially small probability of the ordinary inelastic collisions $P(\overline{X}_1 \to \overline{X}_0)d\overline{X}_0$. Although Kuninaka and Hayakawa [69] examined whether the fluctuation theorem was valid for inelastic collisions based on their molecular dynamics simulation, their result did not support the existence of the fluctuation theorem.

Figure 12(a) shows the ratio of time normal to reversal probability distributions $P/\overline{P}$ against the macroscopic energy loss $W(X_0 \to X_1)$ observed in our simulation for $g = 0.2$, where we define $P \equiv P(X_0 \to X_1)$ and $\overline{P} \equiv P(\overline{X}_1 \to \overline{X}_0)$. We take $N_{tot} = 20\,000$ samples at $T = 2.14 \times 10^{-8} M(c^{(t)})^2$ (300 K in the physical unit) and $v_{CM}(0) = 0.009c^{(t)}$, whereas we take $\overline{N}_{tot}$ samples for various initial speeds. $\overline{N}_{tot}$ is larger than 1000, while $\overline{N}_{tot}$ depends on $\overline{X}_1$. We evaluate probabilities P and $\overline{P}$ as

$$P = \frac{N_{eve}}{N_{tot}}, \quad \overline{P} = \frac{\overline{N}_{eve}}{\overline{N}_{tot}}, \tag{19}$$

where N_{eve} and $\overline{N}_{eve}$ are the numbers of events of the transition from fixed $v_{CM}(0) = 0.009c^{(t)}$ into the interval between $v_{CM}(t_f) - \Delta v/2$ and $v_{CM}(t_f) + \Delta v/2$ and the transition from fixed $-v_{CM}(t_f)$ into the interval between $-v_{CM}(0) - \Delta v/2$ and $-v_{CM}(0) + \Delta v/2$, respectively. We adopt the bin width $\Delta v = 10^{-4} v_{CM}(0)$, and N_{eve} and $\overline{N}_{eve}$ are larger than 100 for each bin. Here we assume that the errors of the probabilities

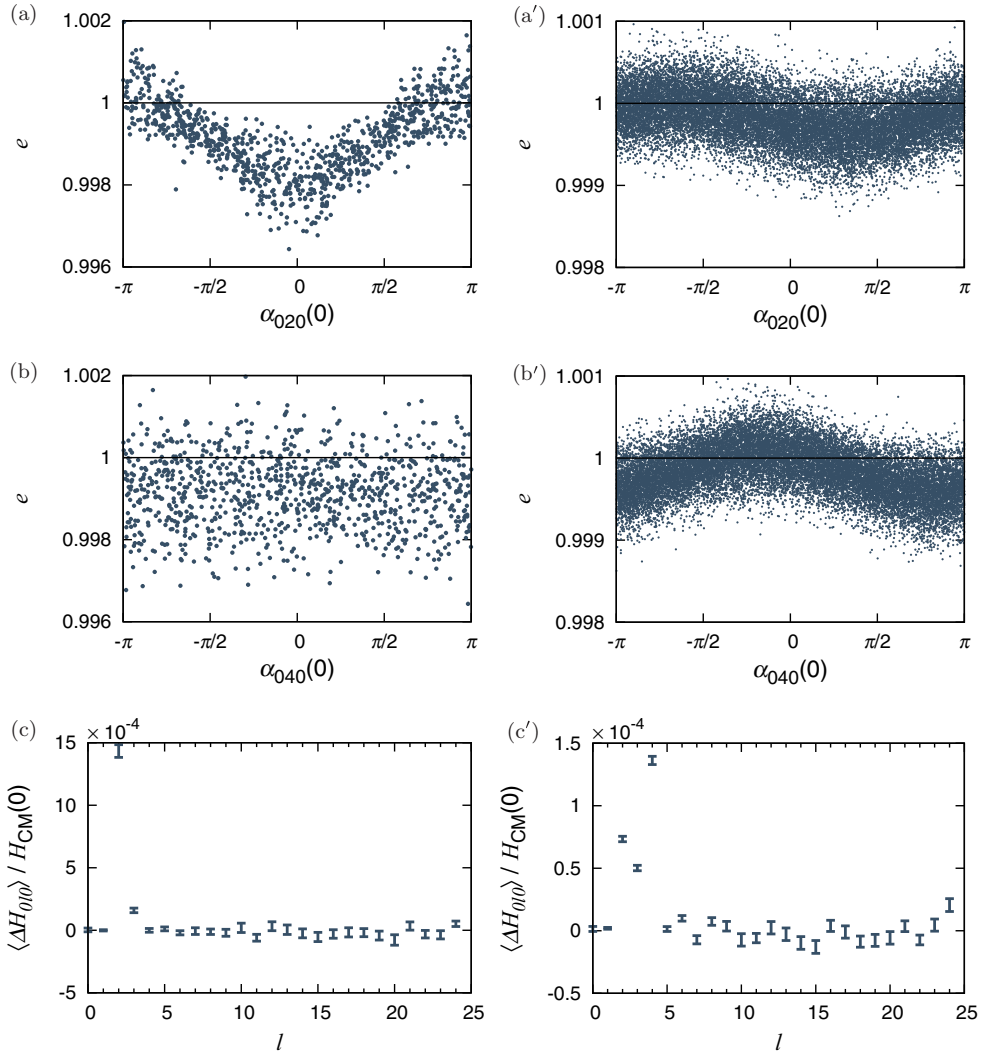

FIG. 11. (Color online) The relation between the restitution coefficient and the initial phase of (a), (a′) the quadrupole ($\ell = 2$) mode and (b), (b′) the 16-pole ($\ell = 4$) mode. We plot in (c) and (c′) the excitation of each fundamental ($n = 0$) and axial ($m = 0$) eigenmode. (a), (b) and (c) are the results for $v_{CM}(0) = 0.007c^{(t)}$ and include 1000 samples, whereas (a′), (b′) and (c′) are the results for $v_{CM}(0) = 0.009c^{(t)}$ and include 20000 samples. The error bar in (c) and (c′) represents the standard deviation.

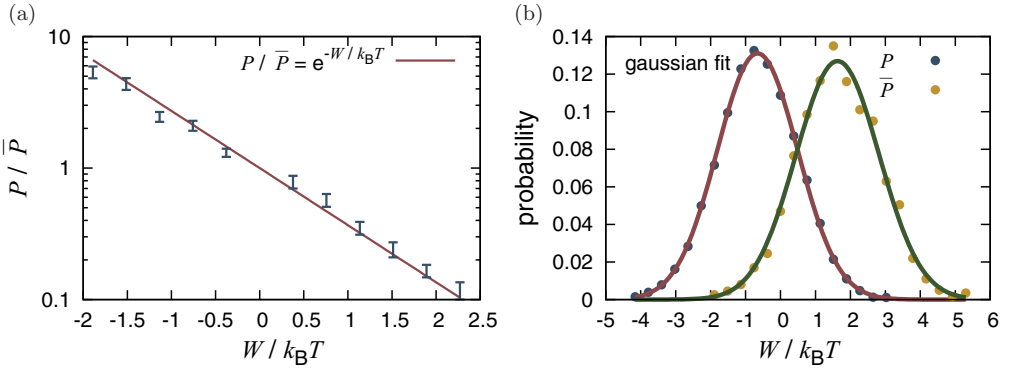

FIG. 12. (Color onine) (a) The relation between $P/\overline{P}$ and W at $T = 2.14 \times 10^{-8} M(c^{(t)})^2$ (300 K in the physical unit) and $v_{CM}(0) = 0.009c^{(t)}$, and (b) the probability distributions P and $\overline{P}$ against W/k_BT, in which the initial speeds are $0.009c^{(t)}$ and $0.0090054c^{(t)}$, respectively.

are given by

$$\sigma_{\rm err}^{(P)} = \frac{\sqrt{N_{\rm eve}}}{N_{\rm tot}}, \quad \sigma_{\rm err}^{(\overline{P})} = \frac{\sqrt{\overline{N}_{\rm eve}}}{\overline{N}_{\rm tot}}. \tag{20}$$

Considering the propagation of error, we also assume that the error of the ratio $P/\overline{P}$ is given by

$$\sigma_{\rm err}^{(P/\overline{P})} = \frac{P}{\overline{P}}\sqrt{\left(\frac{\sigma_{\rm err}^{(P)}}{P}\right)^2 + \left(\frac{\sigma_{\rm err}^{(\overline{P})}}{\overline{P}}\right)^2} = \frac{P}{\overline{P}}\sqrt{\frac{1}{N_{\rm eve}} + \frac{1}{\overline{N}_{\rm eve}}}, \tag{21}$$

The error bars in Fig. 12(a) are calculated from Eq. (21), and the solid line represents the theoretical prediction (18), which is in good agreement with our simulation results. This is the first numerical verification of the extended fluctuation theorem for inelastic collisions.

Figure 12(b) exhibits the probability distributions P and $\overline{P}$, in which the initial speeds are $0.009c^{(\rm t)}$ and $0.0090054c^{(\rm t)}$, respectively. These distributions can be fitted by the Gaussians. The extended fluctuation theorem proposed by Tasaki [55] is reasonable because our model described by Eqs. (1) and (7) assumes the separation between the translational mode and the other internal modes. This separation may not be satisfied in collisions based on the molecular dynamics simulation [69].

C. Heating during collisions

Our basic Eq. (2) assumes that the colliding spheres are in an isothermal state, where the collisional heating can be ignored. To verify its validity, we estimate the amount of heating up during collisions. It is known that the heating in linear elasticity $\Delta T(t;\boldsymbol{x})$ is proportional to the initial temperature of elastic spheres T and the trace of strain tensor $\nabla\cdot\boldsymbol{u}(t;\boldsymbol{x})$ [70,71]

$$\Delta T(t;\boldsymbol{x}) = -T\frac{3K_{\rm ad}\alpha}{c_P}\nabla\cdot\boldsymbol{u}(t;\boldsymbol{x}), \tag{22}$$

where α and c_P are the coefficient of linear expansion and the specific heat capacity at constant pressure, and the adiabatic modulus $K_{\rm ad}$ is related to the bulk modulus K as

$$\frac{1}{K_{\rm ad}} = \frac{1}{K} - \frac{9T\alpha^2}{c_P}. \tag{23}$$

Figure 13 shows the heating distribution on the cross section at the instant of the impact with the large impact speed

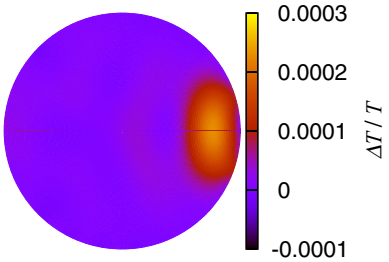

FIG. 13. (Color online) The heating distribution on the cross section at the instant of the impact for $v_{\rm CM} = 0.1$. It should be noted that the heat distribution is plotted at the position of an undeformed sphere.

$v_{\rm CM} = 0.1$ within our framework for isothermal calculation, where we use parameters for copper $\alpha = 16.5\times10^{-6}$/K and $c_P = 24.5$ J/mol K, and $T = 2.14\times10^{-8}M(c^{(\rm t)})^2$ (300 K in the physical unit). Although we observe a little heating with the order $\Delta T/T < 10^{-4}$, this small increment of the temperature is negligible, which is consistent with the isothermal assumption. Therefore, we believe that our calculation can be used even for relatively high speed impacts.

V. DISCUSSION

Now let us discuss our results. In the first part of Sec. V A we develop the perturbation theory to explain the rebound processes. In the second part (Sec. V B) we discuss the mode transfer starting from one mode excitation state. In the last part (Sec. V C) we discuss future problems and perspectives.

A. Perturbation theory

In this section, we examine the perturbation theory of this system to understand the sinusoidal structure of the restitution coefficient against the initial phase [see Fig. 11(a)]. Here we restrict our interest to the perfectly elastic case $\gamma = 0$ at $T = 0$, though we can easily extend our theory to the dissipative case, i.e., $\gamma > 0$ and finite T.

For the perfectly elastic case, the energy conservation law leads to the simple relation for the restitution coefficient

$$e^2 = 1 - \sum_{i,n\ell m}\frac{\Delta H_{i,n\ell m}}{H_{\rm CM}(0)}. \tag{24}$$

Thus, if we know the excitation $\Delta H_{i,n\ell m}$, we can determine the restitution coefficient e.

First, we assume that the time evolutions of the center of mass $z_{\rm CM}(t)$ and the vibrational mode $Q_{n\ell m}(t)$ are scaled by $t_{\rm CM}\equiv R_{\rm eff}/v_{\rm CM}(0)$ and $t_{\rm vib}\equiv R_{\rm eff}/c^{(\rm t)}$, respectively. We introduce dimensionless variables using these time units and the reduced radius $R_{\rm eff}$ and mass $M_{\rm eff}$. Then, equations of motion (1) and (7) are rewritten as

$$\frac{d^2\tilde{z}_{\rm CM}}{d\tilde{t}_{\rm CM}^2} + \frac{\partial\tilde{V}(\tilde{z}_{\rm CM},\{\tilde{Q}_{i',n'\ell'm'}\})}{\partial\tilde{z}_{\rm CM}} = 0, \tag{25}$$

$$\frac{d^2\tilde{Q}_{i,n\ell m}}{d\tilde{t}_{\rm vib}^2} + \tilde{\omega}_{i,n\ell}^2\tilde{Q}_{i,n\ell m} = -\varepsilon^2\frac{1}{\tilde{M}_i}\frac{\partial\tilde{V}(\tilde{z}_{\rm CM},\{\tilde{Q}_{i',n'\ell'm'}\})}{\partial\tilde{Q}_{i,n\ell m}}, \tag{26}$$

where $\tilde{z}_{\rm CM}\equiv z_{\rm CM}/R_{\rm eff}$, $\tilde{Q}_{i,n\ell m}\equiv Q_{n\ell m}/R_{\rm eff}$, $\tilde{t}_{\rm CM}\equiv t/t_{\rm CM}$, $\tilde{t}_{\rm vib}\equiv t/t_{\rm vib}$, $\tilde{\omega}_{i,n\ell}\equiv\omega_{n\ell}t_{\rm vib}$, $\tilde{M}_i\equiv M_i/M_{\rm eff}$, and $\tilde{V}[\tilde{z}_{\rm CM},\{\tilde{Q}_{i,n\ell m}\}]\equiv V[z_{\rm CM}(t),\{Q_{n\ell m}(t)\}]/M_{\rm eff}v_{\rm CM}(0)^2$ are dimensionless variables. Here we introduce the expansion parameter $\varepsilon\equiv v_{\rm CM}(0)/c^{(\rm t)}$, and expand $\tilde{z}_{\rm CM}$ and $\tilde{Q}_{i,n\ell m}$ as

$$\tilde{Q}_{i,n\ell m} = \tilde{Q}_{i,n\ell m}^{(0)} + \varepsilon\tilde{Q}_{i,n\ell m}^{(1)} + \varepsilon^2\tilde{Q}_{i,n\ell m}^{(2)} + \cdots, \tag{27}$$

$$\tilde{z}_{\rm CM} = \tilde{z}_{\rm CM}^{(0)} + \varepsilon\tilde{z}_{\rm CM}^{(1)} + \varepsilon^2\tilde{z}_{\rm CM}^{(2)} + \cdots, \tag{28}$$

where $\tilde{z}_{\rm CM}^{(j)}$ and $\tilde{Q}_{i,n\ell m}^{(j)}$ are the jth order expansion coefficients. We adopt that these coefficients are initially zero except for unperturbed coefficients, i.e., $\tilde{z}_{\rm CM}(0) = \tilde{z}_{\rm CM}^{(0)}(0)$ and $\tilde{Q}_{i,n\ell m}(0) = \tilde{Q}_{i,n\ell m}^{(0)}(0)$. Then, the unperturbed equations are

given by

$$\frac{d^2\tilde{z}^{(0)}_{\rm CM}}{d\tilde{t}^2_{\rm CM}} + \frac{\partial\tilde{V}\left(\tilde{z}^{(0)}_{\rm CM},0\right)}{\partial\tilde{z}_{\rm CM}} = 0, \tag{29}$$

$$\frac{d^2\tilde{Q}^{(0)}_{i,n\ell m}}{d\tilde{t}^2_{\rm vib}} + \tilde{\omega}^2_{i,n\ell}\tilde{Q}^{(0)}_{i,n\ell m} = 0, \tag{30}$$

where we have assumed that $\{\tilde{Q}^{(0)}_{i,n\ell m}\}$ is negligible in the potential V to be consistent with the linear theory of elasticity. The solution of Eq. (29) is immediately given by

$$\tilde{t}_{\rm CM} = \begin{cases} \int_{\tilde{z}^{(0)}_{\rm CM}(0)}^{\tilde{z}^{(0)}_{\rm CM}} \frac{dx}{\sqrt{1-2\tilde{V}(x,0)}} & \left(\tilde{t}_{\rm CM} \leqslant \tilde{t}^{\rm col}_{\rm CM}\right), \\ \int_{\tilde{z}^{(0)}_{\rm CM}(0)}^{\tilde{z}^{\rm col}_{\rm CM}} \frac{dx}{\sqrt{1-2\tilde{V}(x,0)}} - \int_{\tilde{z}^{\rm col}_{\rm CM}}^{\tilde{z}^{(0)}_{\rm CM}} \frac{dx}{\sqrt{1-2\tilde{V}(x,0)}} & \left(\tilde{t}_{\rm CM} > \tilde{t}^{\rm col}_{\rm CM}\right), \end{cases} \tag{31}$$

where $\tilde{z}^{\rm col}_{\rm CM} \equiv \tilde{z}^{(0)}_{\rm CM}(\tilde{t}^{\rm col}_{\rm CM})$ are determined by the condition $1 - 2\tilde{V}(\tilde{z}^{\rm col}_{\rm CM},0) = 0$. From Eq. (30) $\tilde{Q}^{(0)}_{i,n\ell m}$ is just a solution of the equation for a harmonic oscillator. The first order $\tilde{Q}^{(1)}_{i,n\ell m}$ is always zero because $\tilde{Q}^{(1)}_{i,nlm}$ satisfies the equation of the harmonic oscillator under the initial condition we introduced. The second-order equation for the internal vibration is

$$\frac{d^2\tilde{Q}^{(2)}_{i,n\ell m}}{d\tilde{t}^2_{\rm vib}} + \tilde{\omega}^2_{i,n\ell}\tilde{Q}^{(2)}_{i,n\ell m} = -\frac{1}{\tilde{M}_i}\frac{\partial\tilde{V}\left(\tilde{z}^{(0)}_{\rm CM},0\right)}{\partial\tilde{Q}_{i,n\ell m}}, \tag{32}$$

where we also ignore $\{\tilde{Q}^{(0)}_{i,n\ell m}\}$ in the potential V. The solution $\tilde{Q}^{(2)}_{i,n\ell m}$ of Eq. (32) is given by

$$\tilde{Q}^{(2)}_{i,n\ell m}(\tilde{t}_{\rm vib}) = -\frac{1}{\tilde{M}_i\tilde{\omega}_{i,n\ell}}\int_0^{\tilde{t}_{\rm vib}} dt' \frac{\partial\tilde{V}\left(\tilde{z}^{(0)}_{\rm CM}(t'),0\right)}{\partial\tilde{Q}_{i,n\ell m}} \times \sin\tilde{\omega}_{i,n\ell}(\tilde{t}_{\rm vib} - t'). \tag{33}$$

Therefore, the vibrational energy coefficients $\tilde{H}^{(2)}_{i,n\ell m} = \dot{\tilde{Q}}^{(0)}_{i,n\ell m}\dot{\tilde{Q}}^{(2)}_{i,n\ell m} + \tilde{\omega}^2_{i,n\ell}\tilde{Q}^{(0)}_{i,n\ell m}\tilde{Q}^{(2)}_{i,n\ell m}$ and $\tilde{H}^{(4)}_{i,n\ell m} = (\dot{\tilde{Q}}^{(2)}_{i,n\ell m})^2/2 + (\tilde{\omega}_{i,n\ell}\tilde{Q}^{(2)}_{i,n\ell m})^2/2$ are, respectively, reduced to

$$\tilde{H}^{(2)}_{i,n\ell m}(\tilde{t}_{\rm vib}) = -2\sqrt{\tilde{H}^{(0)}_{i,n\ell m}(0)\tilde{H}^{(4)}_{i,n\ell m}(\tilde{t}_{\rm vib})} \times \cos[\alpha_{i,n\ell m}(0) + \tilde{\omega}_{i,n\ell}\tilde{t}_{\rm vib} - \beta_{i,n\ell m}(\tilde{t}_{\rm vib})] \tag{34}$$

$$\tilde{H}^{(4)}_{i,n\ell m}(\tilde{t}_{\rm vib}) = \frac{1}{2\tilde{M}_i^2}\left|\int_0^{\tilde{t}_{\rm vib}} dt' \frac{\partial\tilde{V}\left(\tilde{z}^{(0)}_{\rm CM}(t'),0\right)}{\partial\tilde{Q}_{i,n\ell m}} e^{i\tilde{\omega}_{i,n\ell}t'}\right|^2, \tag{35}$$

where $\beta_{i,n\ell m}(\tilde{t}_{\rm vib})$ is determined by (see Appendix F)

$$\sin\beta_{i,n\ell m}(\tilde{t}_{\rm vib}) = -\frac{\tilde{\omega}_{i,n\ell}\tilde{Q}^{(2)}_{i,n\ell m}(\tilde{t}_{\rm vib})}{\sqrt{2\tilde{H}^{(4)}_{i,n\ell m}(\tilde{t}_{\rm vib})}}, \qquad \cos\beta_{i,n\ell m}(\tilde{t}_{\rm vib}) = -\frac{\dot{\tilde{Q}}^{(2)}_{i,n\ell m}(\tilde{t}_{\rm vib})}{\sqrt{2\tilde{H}^{(4)}_{i,n\ell m}(\tilde{t}_{\rm vib})}}. \tag{36}$$

From Eqs. (24), (34), and (F6), we obtain the sinusoidal behavior of the restitution coefficient against the initial phase $\alpha_{i,n\ell m}(0)$

$$\begin{aligned} e^2 &= 1 + 4\sum_{i,n\ell m}\sqrt{\tilde{H}^{(0)}_{i,n\ell m}(0)\tilde{H}^{(4)}_{i,n\ell m}(t_f)} \times \cos\left(\alpha_{i,n\ell m}(0) + \frac{\tilde{\omega}_{i,n\ell}t_f}{2}\right) + O(\varepsilon^2) \\ &= 1 + 2\sqrt{2}\sum_{i,n\ell m}\sqrt{\tilde{H}^{(4)}_{i,n\ell m}(t_f)}\dot{\tilde{Q}}^{(0)}_{i,n\ell m}(t_f/2) + O(\varepsilon^2), \end{aligned} \tag{37}$$

where t_f is the duration of the interaction. Equation (37) implies that the restitution coefficient can exceed unity if $\dot{\tilde{Q}}^{(0)}_{i,n\ell m}(t_f/2) > 0$ or the sphere expands to the axial direction at the instant $t_f/2$, where the amplitude is proportional to the square root of the excitation energy $\sqrt{\tilde{H}^{(4)}_{i,n\ell m}(t_f)}$.

Finally, we compare this perturbation theory with our simulation to verify the validity of the theory. First, we numerically solve Eq. (29), and then use Eq. (32) to obtain the perturbative solution. Figure 14 exhibits the time evolution of the quadrupole mode energy $\tilde{H}_{n\ell m}$ for Fig. 14(a) $\epsilon = 10^{-3}$ and Fig. 14(b) $\epsilon = 10^{-4}$, where we restrict our interest to the case that the interaction is only characterized by repulsion force. We find that these are in good agreement with each other. The agreements are also found in the other eigenmodes.

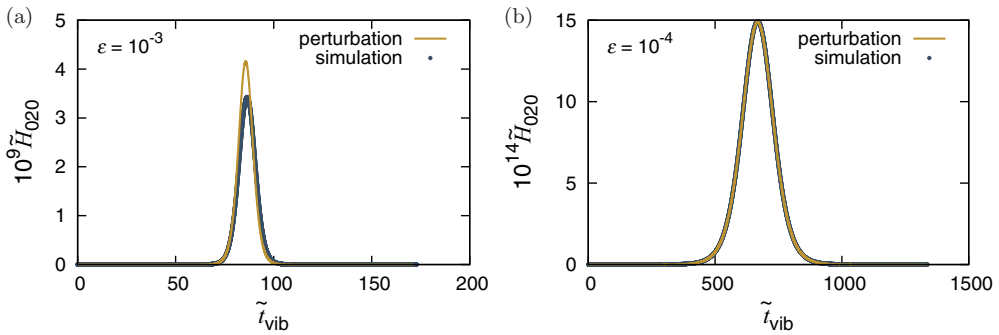

FIG. 14. (Color online) The time evolutions of the quadrupole mode energy $\tilde{H}_{n\ell m}$ for (a) $\epsilon = 10^{-3}$ and (b) $\epsilon = 10^{-4}$, respectively.

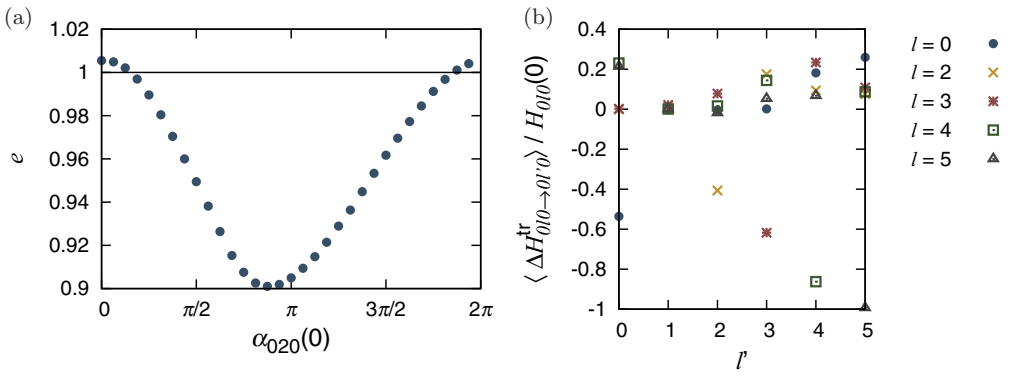

FIG. 15. (Color online) (a) The restitution coefficient as a function of the initial phase of the quadrupole mode and (b) phase-averaged mode transfer $\langle \Delta H^{\rm tr}_{0\ell 0\to 0\ell' 0}\rangle / H_{0\ell 0}(0)$ with fixing $v_{\rm CM}(0) = 0.1c^{(\rm t)}$ and $H_{0\ell 0}(0) = 0.05 H_{\rm CM}(0)$.

Note that our perturbation results fail to reproduce our simulation results even for small ϵ if there exists an attractive interaction because the existence of the sticking force affects the unperturbative solution.

B. Mode transfer induced by collisions

In this section we study the mechanism of mode transfer during collisions. We numerically solve Eqs. (1) and (7) under only one mode excited before the collision, and we calculate the subtracted mode transfer $\Delta H^{\rm tr}_{n\ell m\to n'\ell' m'}$:

$$\Delta H^{\rm tr}_{n\ell m\to n'\ell' m'} \equiv \Delta H_{n\ell m\to n'\ell' m'} - \Delta H_{n'\ell' m'}, \qquad (38)$$

where mode numbers with and without primes represent the final and the initial excited modes, respectively. Here, $\Delta H_{n'\ell' m'}$ and $\Delta H_{n\ell m\to n'\ell' m'}$ are, respectively, the energy transfer at $T = 0$ and the energy transfer with the initial excitation of the (n,ℓ,m) mode. Note that the restitution coefficient depends on the initial phase as well as the initial excitation mode. Figure 15(a) shows the restitution coefficient against the initial phase of the quadrupole mode for the initial speed $v_{\rm CM}(0) = 0.1c^{(\rm t)}$ and the initial excitation energy of this mode $H_{020}(0) = 0.05 H_{\rm CM}(0)$. The superrebound processes for $e > 1$ can be found for small $\alpha_{020}(0)$. Here we investigate the phase-averaged mode transfer to avoid the initial phase dependence

$$\left\langle \Delta H^{\rm tr}_{n\ell m\to n'\ell' m'}\right\rangle_{\alpha_{n\ell m}} \equiv \frac{1}{2\pi}\int_0^{2\pi} d\alpha_{n\ell m}\Delta H^{\rm tr}_{n\ell m\to n'\ell' m'}. \qquad (39)$$

Figure 15(b) shows $\langle \Delta H^{\rm tr}_{0\ell 0\to 0\ell' 0}\rangle / H_{0\ell 0}(0)$ for $v_{\rm CM}(0) = 0.1c^{(\rm t)}$ and $H_{0\ell 0}(0) = 0.05 H_{\rm CM}(0)$. The large negative value in the diagonal elements means that the initial excitation energy is transferred into the other modes. We also find that the off-diagonal elements just nearby the diagonal elements are larger than the other off-diagonal elements, which suggests that the excitation energy transfer between the nearest neighbor mode. We find that the breathing mode ($\ell = 0$) is strongly coupled with the 16-pole ($\ell = 4$) and 32-pole ($\ell = 5$) the eigenfrequencies of which are nearly equal to that of the breathing mode. The dipole mode ($\ell = 1$) is decoupled with any other modes (the diagonal element is positive or nearly equal to zero), though its eigenfrequency is nearly equal to that of the octopole mode. These results are also observed for $v_{\rm CM}(0) = 0.01c^{(\rm t)}$.

C. Future perspectives

In this section, we briefly summarize the future perspectives of our study. Although we restrict our interest to the case of normal head-on collisions of viscoelastic spheres in this paper, there are various interesting phenomena for oblique collisions. For example, Saitoh *et al.* performed the molecular dynamics simulation of the oblique collision between nanoclusters and found that the restitution coefficient becomes negative for large incident angles [25]. In this anomalous collision, it is essential that the duration of contact is finite for nanocluster collisions. To describe oblique collisions in terms of our model, we need to add the torsional modes, though the friction coefficient is necessary in the extension of the macroscopic model.

Although we only adopt the linear theory of elasticity for colliding spheres, nonlinear effects including plastic deformation and fragmentation also play crucial roles in understanding the physics of collisions. In particular, the structural phase transition caused by high speed collisions would be important in understanding the physical mechanism of plastic deformation and fragmentation [17,59]. Needless to say, the nonlinearity becomes dominant for fast collisions in which the impact speed is comparable to the sound speed of colliding bodies.

VI. CONCLUSION

In this paper, we have performed the simulation of head-on collisions based on an isothermal viscoelastic model. We have investigated the restitution coefficient against the impact speed, ranging from slow $0.001c^{(\rm t)}$ to $0.4c^{(\rm t)}$, and found the oscillatory behavior in their relationship if the solid viscosity is sufficiently small. We have confirmed that the oscillation arises from the combination of the contact duration and the eigenfrequencies of the elastic sphere. This oscillation disappears as the solid viscosity is strong.

We have also investigated collisions between a thermally activated elastic sphere and a flat wall. When the impact speed of the colliding sphere is nearly equal to or slower than the thermal speed, we have confirmed the existence of superrebounds if the attraction is reduced. We have confirmed the existence of the fluctuation theorem for collisions of thermal activated spheres. We have also found the sinusoidal structure of the restitution coefficient as a function of the initial

phase of the eigenmodes. This oscillation can be understood by the perturbation theory if there is no attractive force between the sphere and the wall.

ACKNOWLEDGMENTS

We thank M. Sano, H. Kuninaka, K. Saitoh, and F. Kun for helpful discussion, and T. W. Kranz for his introduction of Ref. [58]. This work is partially supported by the Grant-in-Aid of MEXT (Grant No. 25287098).

APPENDIX A: VISCOELASTIC WAVE EQUATION

In this Appendix, we derive the viscoelastic wave equation of isothermal spheres (2) without the external potential. First, let us consider the free energy density within the framework of the linear theory of elasticity [67]

$$f(T,u) = f_0(T) - K(T - T_0)\alpha_{ij}u_{ij} + \tfrac{1}{2}\lambda_{ijkl}u_{ij}u_{kl}, \quad \text{(A1)}$$

where K is the bulk modulus, α_{ij} is the coefficient of thermal expansion, λ_{ijkl} is the elastic modulus tensor, and u_{ij} is the strain tensor

$$u_{ij} = \tfrac{1}{2}(\partial_i u_j + \partial_j u_i). \quad \text{(A2)}$$

The first term on the right-hand side of Eq. (A1) is independent of the elastic deformation u_{ij}. The second term on the right-hand side represents free thermal expansion of the sphere from a base state at the temperature T_0. We ignore this effect in our simulation because the heat up caused by a collision is small (see Sec. IV C). For isotropic spheres, the elastic modulus tensor is given by

$$\lambda_{ijkl} = \lambda\delta_{ij}\delta_{kl} + \mu(\delta_{ik}\delta_{jl} + \delta_{il}\delta_{jk}), \quad \text{(A3)}$$

where λ and μ are Lamé coefficients.

Thus, the free energy of isothermal elastic spheres is reduced to

$$f(T,u) = f_0(T) + \left(\tfrac{1}{2}\lambda u_{ii}u_{jj} + \mu u_{ij}u_{ij}\right). \quad \text{(A4)}$$

Here, the stress tensor $\sigma_{ij}^{\rm el}$ is given by

$$\sigma_{ij}^{\rm el} = \left(\frac{\partial f(T,u)}{\partial u_{ij}}\right)_T = \lambda\delta_{ij}u_{kk} + 2\mu u_{ij}. \quad \text{(A5)}$$

Here we also consider the dissipative stress tensor $\sigma_{ij}^{\rm dis}$ for isotropic bodies [67]

$$\sigma_{ij}^{\rm dis} = \lambda'\frac{\partial}{\partial t}\delta_{ij}\partial_k u_k + \mu'\frac{\partial}{\partial t}(\partial_i u_j + \partial_j u_i), \quad \text{(A6)}$$

where λ' and μ' are the solid viscosity coefficients. Then the equation of the deformation is written as

$$\begin{aligned}\rho\frac{\partial^2 u_i}{\partial t^2} &= \partial_j\left(\sigma_{ij}^{\rm el} + \sigma_{ij}^{\rm dis}\right)\\ &= \left\{\lambda + \mu + (\lambda' + \mu')\frac{\partial}{\partial t}\right\}\partial_i\partial_j u_j + \left(\mu + \mu'\frac{\partial}{\partial t}\right)\partial_j^2 u_i,\end{aligned} \quad \text{(A7)}$$

or

$$\begin{aligned}\frac{\partial^2 \boldsymbol{u}}{\partial t^2} &= \left(\frac{\lambda+\mu}{\rho} + \frac{\lambda'+\mu'}{\rho}\frac{\partial}{\partial t}\right)\boldsymbol{\nabla}\boldsymbol{\nabla}\cdot\boldsymbol{u} + \left(\frac{\mu}{\rho} + \frac{\mu'}{\rho}\frac{\partial}{\partial t}\right)\boldsymbol{\nabla}^2\boldsymbol{u}\\ &= (c^{(\ell)})^2\left(1 + \gamma^{(\ell)}\frac{\partial}{\partial t}\right)\boldsymbol{\nabla}\boldsymbol{\nabla}\cdot\boldsymbol{u}\\ &\quad - (c^{(\mathrm{t})})^2\left(1 + \gamma^{(\mathrm{t})}\frac{\partial}{\partial t}\right)\boldsymbol{\nabla}\times(\boldsymbol{\nabla}\times\boldsymbol{u}).\end{aligned} \quad \text{(A8)}$$

We have introduced

$$c^{(\ell)} = \sqrt{\frac{\lambda+2\mu}{\rho}}, \quad \text{(A9)}$$

$$c^{(\mathrm{t})} = \sqrt{\frac{\mu}{\rho}}, \quad \text{(A10)}$$

and

$$\gamma^{(\ell)} \equiv \frac{\lambda'+2\mu'}{\lambda+2\mu}, \quad \text{(A11)}$$

$$\gamma^{(\mathrm{t})} \equiv \frac{\mu'}{\mu}. \quad \text{(A12)}$$

APPENDIX B: STRESS-FREE SOLUTIONS OF VISCOELASTIC SPHERES

In this Appendix, we solve the wave equation (A8) which is equivalent to Eq. (2) of viscoelastic spheres under stress-free conditions. We now look for a special solution of the form

$$\boldsymbol{u}(t,\boldsymbol{x}) = e^{st}\tilde{\boldsymbol{u}}(\boldsymbol{x}), \quad \text{(B1)}$$

where s is a complex number, corresponding to the Laplace transform without the effect of the initial condition. Substituting Eq. (B1) into Eq. (A8), we obtain

$$\begin{aligned}s^2\tilde{\boldsymbol{u}} &= (c^{(\ell)})^2(1 + \gamma^{(\ell)}s)\boldsymbol{\nabla}\boldsymbol{\nabla}\cdot\tilde{\boldsymbol{u}}\\ &\quad - (c^{(\mathrm{t})})^2(1 + \gamma^{(\mathrm{t})}s)\boldsymbol{\nabla}\times(\boldsymbol{\nabla}\times\tilde{\boldsymbol{u}}).\end{aligned} \quad \text{(B2)}$$

To solve Eq. (B2), we adopt the Helmholtz decomposition

$$\tilde{\boldsymbol{u}} = \tilde{\boldsymbol{u}}^{(\ell)} + \tilde{\boldsymbol{u}}^{(\mathrm{t})}, \quad \text{(B3)}$$

where $\tilde{\boldsymbol{u}}^{(\ell)}$ and $\tilde{\boldsymbol{u}}^{(\mathrm{t})}$ are rotation-free and divergence-free solutions, respectively,

$$\boldsymbol{\nabla}\times\tilde{\boldsymbol{u}}^{(\ell)} = \boldsymbol{0}, \quad \text{(B4)}$$

$$\boldsymbol{\nabla}\cdot\tilde{\boldsymbol{u}}^{(\mathrm{t})} = 0. \quad \text{(B5)}$$

Therefore, $\tilde{\boldsymbol{u}}^{(\ell)}$ can be represented using one scalar potential $\Phi^{(0)}$ and $\tilde{\boldsymbol{u}}^{(\mathrm{t})}$ two scalar potentials $\Phi^{(1,2)}$ with

$$\tilde{\boldsymbol{u}}^{(\ell)} = \boldsymbol{\nabla}\Phi^{(0)}, \quad \text{(B6)}$$

$$\tilde{\boldsymbol{u}}^{(\mathrm{t})} = \boldsymbol{\nabla}\times(\boldsymbol{x}\Phi^{(1)}) + \boldsymbol{\nabla}\times[\boldsymbol{\nabla}\times(\boldsymbol{x}\Phi^{(2)})]. \quad \text{(B7)}$$

Substituting Eqs. (B6) and (B7) into Eq. (B2), one can easily check that these potentials $\Phi^{(i)}$ satisfy the Helmholtz equation. Therefore, $\Phi^{(i)}$ is given by the product of the spherical Bessel function $j_\ell(k_{n\ell}^{(i)}r)$, where the spherical Neumann function is automatically excluded because of the singularity at the origin,

and the spherical harmonics $Y_{\ell m}(\theta,\varphi)$ in a spherical coordinate system

$$\Phi^{(i)} = \Phi^{(i)}_{n\ell m} = B^{(i)}_{n\ell m} j_\ell\left(k^{(i)}_{n\ell} r\right) Y_{\ell m}(\theta,\varphi), \tag{B8}$$

where $B^{(i)}_{n\ell m}$ are the superposition coefficients, and

$$k^{(\ell)}_{n\ell} \equiv k^{(0)}_{n\ell}, \tag{B9}$$

$$k^{(\mathrm{t})}_{n\ell} \equiv k^{(1)}_{n\ell} = k^{(2)}_{n\ell}. \tag{B10}$$

Here, $k^{(\ell)}_{n\ell}$ and $k^{(\mathrm{t})}_{n\ell}$, respectively, satisfy the dispersion relations

$$-s^2_{n\ell} = \left(c^{(\ell)} k^{(\ell)}_{n\ell}\right)^2 (1+\gamma^{(\ell)} s_{n\ell}), \tag{B11}$$

$$-s^2_{n\ell} = \left(c^{(\mathrm{t})} k^{(\mathrm{t})}_{n\ell}\right)^2 (1+\gamma^{(\mathrm{t})} s_{n\ell}). \tag{B12}$$

Substituting Eq. (B8) into Eq. (B6) with the aid of the differential equation for the spherical Bessel function, we obtain

$$\begin{aligned}\tilde{\boldsymbol{u}}(\boldsymbol{x}) &= \tilde{\boldsymbol{u}}_{n\ell m}(\boldsymbol{x}) \\ &= \left[B^{(0)}_{n\ell m} \frac{d j_\ell\left(k^{(\ell)}_{n\ell} r\right)}{dr} + B^{(2)}_{n\ell m} \ell(\ell+1) \frac{j_\ell\left(k^{(\mathrm{t})}_{n\ell} r\right)}{r}\right] Y_{\ell m}(\theta,\varphi)\boldsymbol{e}_r \\ &\quad + \left[B^{(0)}_{n\ell m} j_\ell\left(k^{(\ell)}_{n\ell} r\right) + B^{(2)}_{n\ell m} \frac{d\left\{r j_\ell\left(k^{(\mathrm{t})}_{n\ell} r\right)\right\}}{dr}\right] \nabla Y_{\ell m}(\theta,\varphi) \\ &\quad - B^{(1)}_{n\ell m} r j_\ell\left(k^{(\mathrm{t})}_{n\ell} r\right) \boldsymbol{e}_r \times \nabla Y_{\ell m}(\theta,\varphi). \end{aligned} \tag{B13}$$

Note that $\boldsymbol{e}_r$, $\nabla Y_{\ell m}$ and $\boldsymbol{e}_r \times \nabla Y_{\ell m}$ are, respectively, orthogonal to each other.

Here it should be noted that one can reduce the dispersion relations (B11) and (B12) to simpler forms by rewriting the dispersion relations in real and imaginary parts, separately, if

$$0 < \gamma^{(\ell)} < \frac{2}{c^{(\ell)} k^{(\ell)}_{n\ell}}, \quad 0 < \gamma^{(\mathrm{t})} < \frac{2}{c^{(\mathrm{t})} k^{(\mathrm{t})}_{n\ell}}. \tag{B14}$$

The imaginary part of the dispersion relation becomes

$$\left(c^{(\ell)} k^{(\ell)}_{n\ell}\right)^2 \gamma^{(\ell)} = \left(c^{(\mathrm{t})} k^{(\mathrm{t})}_{n\ell}\right)^2 \gamma^{(\mathrm{t})}, \tag{B15}$$

and the real part of the dispersion relations with the aid of Eq. (B15) is reduced to

$$c^{(\ell)} k^{(\ell)}_{n\ell} = c^{(\mathrm{t})} k^{(\mathrm{t})}_{n\ell} \equiv \omega_{n\ell}, \tag{B16}$$

where $\omega_{n\ell}$ is the eigenfrequency. From Eqs. (B15) and (B16), we obtain a counterintuitive relation

$$\gamma^{(\ell)} = \gamma^{(\mathrm{t})} \equiv \gamma. \tag{B17}$$

This result is remarkable because there is only one solid viscosity.

Now, let us consider the solution of Eq. (B2) under the stress-free boundary condition

$$(\boldsymbol{F}_r)_i \equiv \frac{x_j}{r} \sigma^{\mathrm{el}}_{ij}(R,\theta,\varphi) = 0. \tag{B18}$$

With the aid of Eq. (A5) we can rewrite $\boldsymbol{F}_r$ as

$$\boldsymbol{F}_r = \lambda \nabla \cdot \boldsymbol{u} \boldsymbol{e}_r + \mu\left(\nabla u_r + \frac{u_r}{r}\boldsymbol{e}_r - \frac{\boldsymbol{u}}{r} + \frac{\partial \boldsymbol{u}}{\partial r}\right). \tag{B19}$$

Substituting Eq. (B13) into Eq. (B19), we find

$$\begin{aligned}\frac{\boldsymbol{F}_r}{\mu} &= \frac{\boldsymbol{F}_{r,n\ell m}}{\mu} \\ &= \left[\left(k^{(\ell)}_{n\ell}\right)^2 B^{(0)}_{n\ell m} a_{n\ell}\left(k^{(\ell)}_{n\ell} r\right)\right. \\ &\quad \left. + \left(k^{(\mathrm{t})}_{n\ell}\right)^2 B^{(2)}_{n\ell m} \ell(\ell+1) b_{n\ell}\left(k^{(\mathrm{t})}_{n\ell} r\right)\right] Y_{\ell m}(\theta,\varphi)\boldsymbol{e}_r \\ &\quad + \left[\left(k^{(\ell)}_{n\ell}\right)^2 B^{(0)}_{n\ell m} b_{n\ell}\left(k^{(\ell)}_{n\ell} r\right)\right. \\ &\quad \left. + \left(k^{(\mathrm{t})}_{n\ell}\right)^2 B^{(2)}_{n\ell m} d_{n\ell}\left(k^{(\mathrm{t})}_{n\ell} r\right)\right] r \nabla Y_{\ell m}(\theta,\varphi) \\ &\quad + \frac{1}{2}\left(k^{(\mathrm{t})}_{n\ell} r\right)^2 B^{(1)}_{n\ell m} b_{n\ell}\left(k^{(\mathrm{t})}_{n\ell} r\right) \boldsymbol{e}_r \times \nabla Y_{\ell m}(\theta,\varphi), \end{aligned} \tag{B20}$$

where

$$a_{n\ell}(x) = 2\frac{d^2 j_\ell(x)}{dx^2} - \frac{\lambda}{\mu} j_\ell(x), \tag{B21}$$

$$b_{n\ell}(x) = 2\frac{d}{dx}\left(\frac{j_\ell(x)}{x}\right), \tag{B22}$$

$$d_{n\ell}(x) = 2x\frac{d^2 j_\ell(x)}{dx^2} + (\ell-1)(\ell+2)\frac{j_\ell(x)}{x}. \tag{B23}$$

The boundary condition (B18) is also reduced to a set of the following equations

$$\boldsymbol{A}\begin{pmatrix}\left(k^{(\ell)}_{n\ell}\right)^2 B^{(0)}_{n\ell m} \\ \left(k^{(\mathrm{t})}_{n\ell}\right)^2 B^{(2)}_{n\ell m}\end{pmatrix} = \boldsymbol{0}, \tag{B24}$$

$$b_{n\ell}\left(k^{(\mathrm{t})}_{n\ell} R\right) B^{(1)}_{n\ell m} = 0, \tag{B25}$$

where

$$\boldsymbol{A} \equiv \begin{pmatrix} a_{n\ell}\left(k^{(\ell)}_{n\ell} R\right) & \ell(\ell+1) b_{n\ell}\left(k^{(\mathrm{t})}_{n\ell} R\right) \\ b_{n\ell}\left(k^{(\ell)}_{n\ell} R\right) & d_{n\ell}\left(k^{(\mathrm{t})}_{n\ell} R\right)\end{pmatrix}. \tag{B26}$$

Thus, there are two types of modes; the spheroidal modes

$$\begin{pmatrix} B^{(0)}_{n\ell m} \\ B^{(2)}_{n\ell m}\end{pmatrix} \neq \boldsymbol{0}, \tag{B27}$$

$$B^{(1)}_{n\ell m} = 0, \tag{B28}$$

and the torsional modes

$$\begin{pmatrix} B^{(0)}_{n\ell m} \\ B^{(2)}_{n\ell m}\end{pmatrix} = \boldsymbol{0}, \tag{B29}$$

$$B^{(1)}_{n\ell m} \neq 0. \tag{B30}$$

Therefore, the solution of the spheroidal mode is given by

$$\tilde{\boldsymbol{u}}^{(\mathrm{S})}_{n\ell m}(\boldsymbol{x}) = \left[B^{(0)}_{n\ell m} \frac{d j_\ell\left(k^{(\ell)}_{n\ell} r\right)}{dr} + B^{(2)}_{n\ell m} \ell(\ell+1) \frac{j_\ell\left(k^{(\mathrm{t})}_{n\ell} r\right)}{r} \right] Y_{\ell m}(\theta,\varphi)\boldsymbol{e}_r + \left[B^{(0)}_{n\ell m} j_\ell\left(k^{(\ell)}_{n\ell} r\right) + B^{(2)}_{n\ell m} \frac{d\left\{ r j_\ell\left(k^{(\mathrm{t})}_{n\ell} r\right)\right\}}{dr} \right] \nabla Y_{\ell m}(\theta,\varphi). \quad \text{(B31)}$$

The eigenfrequency $\omega_{n\ell}$ is obtained from $\det \boldsymbol{A} = 0$, and the ratio $B^{(0)}_{n\ell m}/B^{(2)}_{n\ell m}$ is determined by Eq. (B24). Using the remaining freedom, we normalize $\tilde{\boldsymbol{u}}^{(\mathrm{S})}_{n\ell m}(\boldsymbol{x})$

$$\int_0^R dr r^2 \int_0^\pi d\theta \sin\theta \int_0^{2\pi} d\varphi \left|\tilde{\boldsymbol{u}}^{(\mathrm{S})}_{n\ell m}(\boldsymbol{x})\right|^2 = \frac{4\pi}{3} R^3. \quad \text{(B32)}$$

APPENDIX C: FLUCTUATIONS IN CONTINUUM DYNAMICS

As mentioned in the Introduction, the solid viscosity should be associated with the random noise term to satisfy the fluctuation-dissipation relation. In this Appendix, we briefly summarize the form of the fluctuating dissipative stress tensor which represents the random noise in the stress. We also estimate the critical solid viscosity at which the relaxation time originated from the solid viscosity is comparable to the duration of contact.

Here, we assume that the dissipative stress tensor $\sigma^{\mathrm{dis}}_{ij}$ is given by Eq. (A6). In the presence of fluctuations, however, there is fluctuating local stress $\delta\sigma^{\mathrm{dis}}_{ij}$. Thus the dissipative stress is replaced by

$$\sigma^{\mathrm{dis}}_{ij} \to \sigma^{\mathrm{dis}}_{ij} + \delta\sigma^{\mathrm{dis}}_{ij}. \quad \text{(C1)}$$

As in the case of the fluctuating hydrodynamics, the fluctuating stress satisfies the relations

$$\left\langle \delta\sigma^{\mathrm{dis}}_{ij}(t;\boldsymbol{x}) \right\rangle = 0, \quad \text{(C2)}$$

and [72]

$$\left\langle \delta\sigma^{\mathrm{dis}}_{ij}(t_1;\boldsymbol{x}_1)\delta\sigma^{\mathrm{dis}}_{k\ell}(t_2;\boldsymbol{x}_2) \right\rangle = 2T\{2\mu'(\delta_{ik}\delta_{j\ell} + \delta_{i\ell}\delta_{jk}) + \lambda'\delta_{ij}\delta_{k\ell}\}\delta(t_1 - t_2)\delta(\boldsymbol{x}_1 - \boldsymbol{x}_2), \quad \text{(C3)}$$

where we denote the statistical average by $\langle\rangle$.

Although we have introduced the fluctuating local stress in Eq. (C1), it is not important for collisions for small γ. Here we identify the spontaneous relaxation time $\tau^{(\mathrm{r})}_{n\ell}$ coupled with γ. From Eq. (B1), $\tau^{(\mathrm{r})}_{n\ell}$ is defined by

$$\tau^{(\mathrm{r})}_{n\ell} \equiv -\frac{1}{\mathrm{Re}[s_{n\ell}]}, \quad \text{(C4)}$$

where $\mathrm{Re}[s_{n\ell}]$ represents the real part of $s_{n\ell}$. The combination of Eqs. (B11), (B16), and (B17) leads to

$$\tau^{(\mathrm{r})}_{n\ell} = \frac{2}{\omega^2_{n\ell}\gamma}. \quad \text{(C5)}$$

On the other hand, the duration of contact in the quasistatic theory is given by [67]

$$\tau_{\mathrm{H}} = 2.87 \left(\frac{M^2_{\mathrm{eff}}}{Y^2_{\mathrm{eff}} R_{\mathrm{eff}} v_{\mathrm{CM}}(0)} \right)^{1/5}. \quad \text{(C6)}$$

It should be noted that $\tau_{\mathrm{H}}[v_{\mathrm{CM}}(0)]$ is nearly equal to the duration of contact of our simulation, ranging from $v_{\mathrm{CM}}(0) = 0.001c^{(\mathrm{t})}$ to $v_{\mathrm{CM}}(0) = 0.4c^{(\mathrm{t})}$. Here we introduce the critical solid viscosity $\gamma^*_{n\ell}$ at which $\tau^{(\mathrm{r})}_{n\ell} = \tau_{\mathrm{H}}$ is satisfied. Thus, we obtain

$$\gamma^*_{n\ell} = \frac{0.7}{\omega^2_{n\ell}} \left(\frac{Y^2_{\mathrm{eff}} R_{\mathrm{eff}} v_{\mathrm{CM}}(0)}{M^2_{\mathrm{eff}}} \right)^{1/5}. \quad \text{(C7)}$$

For the lowest eigenfrequency $\omega_{02} \simeq 2.65c^{(\mathrm{t})}/R_1$ and $v_{\mathrm{CM}}(0) = 0.001c^{(\mathrm{t})}$, the corresponding critical solid viscosity is estimated as

$$\gamma^*_{02} \simeq 0.02 R_1/c^{(\mathrm{t})}, \quad \text{(C8)}$$

when the target is a flat wall. Therefore, the fluctuating stress is negligible for $\gamma \ll 0.02R_1/c^{(\mathrm{t})}$, which is satisfied for most of the cases we have analyzed in this paper.

APPENDIX D: SOME EXPLICIT EXPRESSIONS

In this Appendix, we briefly summarize the explicit form of the distance (4) for the axisymmetric case, and the potential (5) for the hard wall limit, i.e., $c^{(\mathrm{t})}_2 \to \infty$, $c^{(\ell)}_2 \to \infty$ and $R_2 \to \infty$.

1. Distance (4) for the axisymmetric case

To summarize some complicated expressions, we introduce

$$z(z_{\mathrm{CM}},\{Q_{i',n'\ell'm'}\};\theta_1,\varphi_1;\theta_2,\varphi_2) \equiv z_{\mathrm{CM}} - R_2\cos\theta_2 - u_{z2}(\{Q_{2,n'\ell'm'}\};R_2,\theta_2,\varphi_2) - R_1\cos\theta_1 - u_{z1}(\{Q_{1,n'\ell'm'}\};R_1,\theta_1,\varphi_1), \quad \text{(D1)}$$

$$u_{xy} \equiv u_r\cos\theta + u_\theta\sin\theta. \quad \text{(D2)}$$

If the initial excitation of the elastic spheres is absent, the normal head-on collision is axisymmetric, in which $u_\varphi = 0$ and u_{xy} and $z(z_{\mathrm{CM}},\{Q_{i',n'\ell'm'}\};\theta_1,\varphi_1;\theta_2,\varphi_2)$ are independent of both φ_1 and φ_2. Then the distance (4) and its derivative are given by

$$r^2 = \{R_2\sin\theta_2 + u_{xy2}(\{Q_{2,n'\ell'm'}\};R_2,\theta_2)\}^2 + \{R_1\sin\theta_1 + u_{xy1}(\{Q_{1,n'\ell'm'}\};R_1,\theta_1)\}^2 + 2\{R_2\sin\theta_2 + u_{xy2}(\{Q_{2,n'\ell'm'}\};R_2,\theta_2)\}\{R_1\sin\theta_1 + u_{xy1}(\{Q_{1,n'\ell'm'}\};R_1,\theta_1)\}\cos(\varphi_1+\varphi_2) + \{z(z_{\mathrm{CM}},\{Q_{i',n'\ell'm'}\};\theta_1;\theta_2)\}^2, \quad \text{(D3)}$$

$$\frac{1}{2}\frac{\partial r^2}{\partial Q_{1,n\ell m}} = \tilde{u}_{xy,n\ell m}(R_1,\theta_1,\varphi_1)[\{R_2\sin\theta_2 + u_{xy2}(\{Q_{2,n'\ell'm'}\};R_2,\theta_2)\}\cos(\varphi_1+\varphi_2) + \{R_1\sin\theta_1 + u_{xy1}(\{Q_{1,n'\ell'm'}\};R_1,\theta_1)\}]$$
$$- \tilde{u}_{\varphi,n\ell m}(R_1,\theta_1,\varphi_1)\{R_2\sin\theta_2 + u_{xy2}(\{Q_{2,n'\ell'm'}\};R_2,\theta_2)\}\sin(\varphi_1+\varphi_2) - \tilde{u}_{z,n\ell m}(R_1,\theta_1,\varphi_1)z(z_{\rm CM},\{Q_{i',n'\ell'm'}\};\theta_1;\theta_2). \tag{D4}$$

Equation (D3) includes only $\varphi_1+\varphi_2$ and Eq. (D4) includes φ_1 and $\varphi_1+\varphi_2$. In addition, ϕ_1 dependence only appears in the coefficients $\tilde{u}_{xy,n\ell m}$, $\tilde{u}_{\varphi,n\ell m}$, and $\tilde{u}_{z,n\ell m}$ where the integral with respect to ϕ_1 disappears except for $m=0$. Therefore, both $F_{1,n\ell m}$ and $Q_{1,n\ell m}$ for $m\neq 0$ are absent during the axisymmetric collision. For $m=0$, $\tilde{u}_{\varphi,n\ell 0}=0$, and $\tilde{u}_{xy,n\ell 0}$ and $\tilde{u}_{z,n\ell 0}$ is also independent of φ. Thus, Eq. (D4) becomes

$$\frac{1}{2}\frac{\partial r^2}{\partial Q_{1,n\ell 0}} = \tilde{u}_{xy,n\ell 0}(R_1,\theta_1)[\{R_2\sin\theta_2 + u_{xy2}(\{Q_{2,n'\ell'0}\};R_2,\theta_2)\}\cos(\varphi_1+\varphi_2) + \{R_1\sin\theta_1 + u_{xy1}(\{Q_{1,n'\ell'0}\};R_1,\theta_1)\}]$$
$$- \tilde{u}_{z,n\ell}(R_1,\theta_1)z(z_{\rm CM},\{Q_{i',n'\ell'0}\};\theta_1;\theta_2). \tag{D5}$$

$\partial r^2/\partial Q_{1,n\ell 0}$ also depends only on $\varphi_1+\varphi_2$. The integration of $\varphi_1+\varphi_2$ in $F_{1,n\ell m}$ can be excluded analytically, while we avoid writing the complicated result. See the detailed calculation in Ref. [73]

2. Potential (5) for the hard wall limit

In the case of the limitation $c_2^{(\rm t)}\to\infty$, $c_2^{(\ell)}\to\infty$, and $R_2\to\infty$, the potential (5) can be reduced to

$$\begin{aligned} V(z_{\rm CM},\boldsymbol{u}_1) &= 4\epsilon\frac{R_1^2}{d_1^2d_2^2}\int_0^{\pi/2}d\theta_1\sin\theta_1\int_0^{2\pi}d\varphi_1\int_{-\infty}^{\infty}dx_2\int_{-\infty}^{\infty}dy_2 \\ &\quad\times\left[\left(\frac{\sigma}{\sqrt{(x_2-x_1)^2+(y_2-y_1)^2+(z_2-z_1)^2}}\right)^{12} - \left(\frac{\sigma}{\sqrt{(x_2-x_1)^2+(y_2-y_1)^2+(z_2-z_1)^2}}\right)^{6}\right], \\ &= 4\pi\epsilon\frac{R_1^2\sigma^2}{d^4}\int_0^{\pi/2}d\theta_1\sin\theta_1\int_0^{2\pi}d\varphi_1\left[\frac{1}{5}\left(\frac{\sigma}{z_2-z_1}\right)^{10} - \frac{1}{2}\left(\frac{\sigma}{z_2-z_1}\right)^{4}\right], \\ &= 4\pi\epsilon\frac{R_1^2\sigma^2}{d^4}\int_0^{\pi/2}d\theta_1\sin\theta_1\int_0^{2\pi}d\varphi_1 \\ &\quad\times\left[\frac{1}{5}\left(\frac{\sigma}{z_{\rm CM,w}+R_1\cos\theta_1+u_z(R_1,\theta_1,\varphi_1)}\right)^{10} - \frac{1}{2}\left(\frac{\sigma}{z_{\rm CM,w}+R_1\cos\theta_1+u_z(R_1,\theta_1,\varphi_1)}\right)^{4}\right], \end{aligned} \tag{D6}$$

where (x_1,y_1,z_1) and (x_2,y_2,z_2) are the positions on the surface of the sphere and the wall, respectively. We have introduced $z_{\rm CM,w}$ as the distance between the center of mass position of the sphere 1 and the wall, and used polar coordinates to obtain the last equality. Note that the integral $\int\varphi_1$ is just reduced to 2π in Eq. (D6) if the initial vibration is absent but the replacement cannot be used for the initial excited case because $u_z(R_1,\theta_1,\varphi_1)$ depends on φ_1.

APPENDIX E: THIRD TERM ON THE RIGHT-HAND SIDE OF EQ. (14)

Here we explain that the coefficient γ in the third term on the right-hand side of Eq. (14) is identical to that used by Brilliantov *et al.* [29]

$$A=\alpha^2\beta=\left(\frac{\lambda'}{\lambda}\right)^2\frac{3\lambda+2\mu}{3\lambda'+2\mu'}, \tag{E1}$$

where the notation corresponds to Eqs. (A5) and (A6) instead of their notation

$$\sigma_{ij}^{\rm el} = E_1\left(u_{ij}-\tfrac{1}{3}\delta_{ij}u_{kk}\right)+E_2\delta_{ij}u_{kk}, \tag{E2}$$

$$\sigma_{ij}^{\rm dis} = \eta_1\frac{\partial}{\partial t}\left(u_{ij}-\frac{1}{3}\delta_{ij}u_{kk}\right)+\eta_2\frac{\partial}{\partial t}\delta_{ij}u_{kk}. \tag{E3}$$

From Eqs. (A11), (A12), and (B17), we obtain

$$\lambda'=\lambda\gamma, \tag{E4}$$

$$\mu'=\mu\gamma. \tag{E5}$$

Therefore, we finally obtain the relation

$$\gamma = \left(\frac{\lambda'}{\lambda}\right)^2 \frac{3\lambda + 2\mu}{3\lambda' + 2\mu'}. \tag{E6}$$

APPENDIX F: DERIVATION OF EQ. (34)

Here we derive Eq. (34) in Sec. V A. Because the solution of the unperturbed vibrational mode $\tilde{Q}^{(0)}_{i,n\ell m}$ is given by

$$\tilde{Q}^{(0)}_{i,n\ell m}(\tilde{t}_{\rm vib}) = \frac{1}{\tilde{\omega}_{i,n\ell}}\sqrt{2\tilde{H}^{(0)}_{i,n\ell m}(0)}\,\sin[\alpha_{i,n\ell m}(0) + \tilde{\omega}_{i,n\ell}\tilde{t}_{\rm vib}], \tag{F1}$$

the vibrational energy coefficient of the second order $\tilde{H}^{(2)}_{i,n\ell m}(\tilde{t}_{\rm vib})$ becomes

$$\begin{aligned}
\tilde{H}^{(2)}_{i,n\ell m}(\tilde{t}_{\rm vib}) &= \dot{\tilde{Q}}^{(0)}_{i,n\ell m}(\tilde{t}_{\rm vib})\dot{\tilde{Q}}^{(2)}_{i,n\ell m}(\tilde{t}_{\rm vib}) + \tilde{\omega}^2_{i,n\ell}\tilde{Q}^{(0)}_{i,n\ell m}(\tilde{t}_{\rm vib})\tilde{Q}^{(2)}_{i,n\ell m}(\tilde{t}_{\rm vib}) \\
&= \sqrt{2\tilde{H}^{(0)}_{i,n\ell m}(0)}\big\{\dot{\tilde{Q}}^{(2)}_{i,n\ell m}(\tilde{t}_{\rm vib})\cos(\alpha_{i,n\ell m}(0) + \tilde{\omega}_{i,n\ell}\tilde{t}_{\rm vib}) + \tilde{\omega}_{i,n\ell}\tilde{Q}^{(2)}_{i,n\ell m}(\tilde{t}_{\rm vib})\sin(\alpha_{i,n\ell m}(0) + \tilde{\omega}_{i,n\ell}\tilde{t}_{\rm vib})\big\} \\
&= -2\sqrt{\tilde{H}^{(0)}_{i,n\ell m}(0)\tilde{H}^{(4)}_{i,n\ell m}(\tilde{t}_{\rm vib})}\cos[\alpha_{i,n\ell m}(0) + \tilde{\omega}_{i,n\ell}\tilde{t}_{\rm vib} - \beta_{i,n\ell m}(\tilde{t}_{\rm vib})].
\end{aligned} \tag{F2}$$

In the final line, we have used $\tilde{H}^{(4)}_{i,n\ell m} = (\dot{\tilde{Q}}^{(2)}_{i,n\ell m})^2/2 + (\tilde{\omega}_{i,n\ell}\tilde{Q}^{(2)}_{i,n\ell m})^2/2$, and introduced $\beta_{i,n\ell m}(\tilde{t}_{\rm vib})$:

$$\sin\beta_{i,n\ell m}(\tilde{t}_{\rm vib}) = -\frac{\tilde{\omega}_{i,n\ell}\tilde{Q}^{(2)}_{i,n\ell m}(\tilde{t}_{\rm vib})}{\sqrt{2\tilde{H}^{(4)}_{i,n\ell m}(\tilde{t}_{\rm vib})}}, \quad \cos\beta_{i,n\ell m}(\tilde{t}_{\rm vib}) = -\frac{\dot{\tilde{Q}}^{(2)}_{i,n\ell m}(\tilde{t}_{\rm vib})}{\sqrt{2\tilde{H}^{(4)}_{i,n\ell m}(\tilde{t}_{\rm vib})}}. \tag{F3}$$

Because the time evolution of the force $\partial\tilde{V}(\tilde{z}^{(0)}_{\rm CM}(t),0)/\partial\tilde{Q}_{i,n\ell m}$ is symmetric around the instant of the collision $t_f/2$, $\sin\beta_{i,n\ell m}$ at $\tilde{t}_{\rm vib} = t_f$ can be written as

$$\begin{aligned}
\sin\beta_{i,n\ell m}(t_f) &= \frac{\int_0^{t_f} dt' \frac{\partial\tilde{V}(\tilde{z}^{(0)}_{\rm CM}(t'),0)}{\partial\tilde{Q}_{i,n\ell m}}\sin\tilde{\omega}_{i,n\ell}(t_f - t')}{\sqrt{\left|\int_0^{t_f} dt' \frac{\partial\tilde{V}(\tilde{z}^{(0)}_{\rm CM}(t'),0)}{\partial\tilde{Q}_{i,n\ell m}} e^{i\tilde{\omega}_{i,n\ell}t'}\right|^2}} = \frac{\int_{-t_f/2}^{t_f/2} dt' \frac{\partial\tilde{V}(\tilde{z}^{(0)}_{\rm CM}(t_f/2+t'),0)}{\partial\tilde{Q}_{i,n\ell m}}\sin\tilde{\omega}_{i,n\ell}(t_f/2 - t')}{\sqrt{\left|\int_{-t_f/2}^{t_f/2} dt' \frac{\partial\tilde{V}(\tilde{z}^{(0)}_{\rm CM}(t_f/2+t'),0)}{\partial\tilde{Q}_{i,n\ell m}} e^{i\tilde{\omega}_{i,n\ell}t'}\right|^2}} \\
&= \frac{\sin\frac{\tilde{\omega}_{i,n\ell}t_f}{2}\int_{-t_f/2}^{t_f/2} dt' \frac{\partial\tilde{V}(\tilde{z}^{(0)}_{\rm CM}(t_f/2+t'),0)}{\partial\tilde{Q}_{i,n\ell m}}\cos\tilde{\omega}_{i,n\ell}t'}{\left|\int_{-t_f/2}^{t_f/2} dt' \frac{\partial\tilde{V}(\tilde{z}^{(0)}_{\rm CM}(t_f/2+t'),0)}{\partial\tilde{Q}_{i,n\ell m}}\cos\tilde{\omega}_{i,n\ell}t'\right|} = \sin\frac{\tilde{\omega}_{i,n\ell}t_f}{2}.
\end{aligned} \tag{F4}$$

In the final expression, we have removed the absolute value in the denominator because $\partial\tilde{V}(\tilde{z}^{(0)}_{\rm CM}(t),0)/\partial\tilde{Q}_{i,n\ell m}$ is always positive and monotonically increases up to $t = t_f/2$. We can also calculate $\cos\beta_{i,n\ell m}(t_f)$, and the result becomes

$$\cos\beta_{i,n\ell m}(t_f) = \cos\frac{\tilde{\omega}_{i,n\ell}t_f}{2}. \tag{F5}$$

Therefore,

$$\beta_{i,n\ell m}(t_f) = \frac{\tilde{\omega}_{i,n\ell}t_f}{2}. \tag{F6}$$

[1] *Physics of Dry Granular Media*, NATO ASI, edited by H. J. Herrmann, J.-P. Hovi, and S. Luding (Kluwer, Dordrecht, The Netherlands, 1998).

[2] *The Physics of Granular Media*, edited by H. Hinrichsen and D. Wolf (Wiley-VCH, Berlin, 2004).

[3] N. T. Bridges, F. Ayoub, J.-P. Avouac, S. Leprince, A. Lucas, and S. Mattson, Nature (London) **485**, 339 (2012).

[4] P. S. Kumar, V. Keerthi, A. S. Kumar, J. Mustard, B. G. Krishna, Amitabh, L. R. Ostrach, D. A. Kring, A. S. K. Kumar, and J. N. Goswami, J. Geophys. Res. (Planets) **118**, 206 (2013).

[5] S. J. Weidenschilling, Icarus **44**, 172 (1980).

[6] Y. Nakagawa, K. Nakazawa, and C. Hayashi, Icarus **45**, 517 (1981).

[7] H. Tanaka, Y. Himeno, and S. Ida, Astrophys. J. **625**, 414 (2005).

[8] C. P. Dullemond and C. Dominik, A&A **434**, 971 (2005).

[9] F. Brauer, C. P. Dullemond, and T. Henning, A&A **480**, 859 (2008).

[10] H. M. Jaeger, S. R. Nagel, and R. P. Behringer, Rev. Mod. Phys. **68**, 1259 (1996).
[11] A. Castellanos, Adv. Phys. **54**, 263 (2005).
[12] J. Tomas, Chem. Eng. Sci. **62**, 1997 (2007).
[13] J. Tomas, Chem. Eng. Sci. **62**, 5925 (2007).
[14] R. Tykhoniuk, J. Tomas, S. Luding, M. Kappl, L. Heim, and H.-J. Butt, Chem. Eng. Sci. **62**, 2843 (2007).
[15] A. Bertram and J. Tomas, *Micro-Macro-Interactions in Structured Media and Particle Systems* (Springer-Verlag, Berlin, 2008).
[16] F. G. Bridges, A. Hatzes, and D. N. C. Lin, Nature (London) **309**, 333 (1984).
[17] K. L. Johnson, *Contact Mechanics* (Cambridge University Press, Cambridge, England, 1985).
[18] G. Kuwabara and K. Kono, Jpn. J. Appl. Phys. **26**, 1230 (1987).
[19] N. V. Brilliantov, F. Spahn, J.-M. Hertzsch, and T. Pöschel, Phys. Rev. E **53**, 5382 (1996).
[20] W. A. M. Morgado and I. Oppenheim, Phys. Rev. E **55**, 1940 (1997).
[21] M. Y. Louge and M. E. Adams, Phys. Rev. E **65**, 021303 (2002).
[22] H. Kuninaka and H. Hayakawa, Phys. Rev. Lett. **93**, 154301 (2004).
[23] H. Hayakawa and H. Kuninaka, Phase Trans. **77**, 889 (2004).
[24] C. Shen, Y. Wang, S. Wang, Y. Liu, R. Liu, A. Vourlidas, B. Miao, P. Ye, J. Liu, and Z. Zhou, Nat. Phys. **8**, 923 (2012).
[25] K. Saitoh, A. Bodrova, H. Hayakawa, and N. V. Brilliantov, Phys. Rev. Lett. **105**, 238001 (2010).
[26] P. Müller, D. Krengel, and T. Pöschel, Phys. Rev. E **85**, 041306 (2012).
[27] P. Müller, M. Heckel, A. Sack, and T. Pöschel, Phys. Rev. Lett. **110**, 254301 (2013).
[28] A. Awasthi, S. C. Hendy, P. Zoontjens, and S. A. Brown, Phys. Rev. Lett. **97**, 186103 (2006).
[29] N. V. Brilliantov, N. Albers, F. Spahn, and T. Pöschel, Phys. Rev. E **76**, 051302 (2007).
[30] M. Suri and T. Dumitrica, Phys. Rev. B **78**, 081405 (2008).
[31] H. Kuninaka and H. Hayakawa, Phys. Rev. E **79**, 031309 (2009); see also Phys. Rev. Focus **23**, 10 (2009).
[32] S. Kim, Phys. Rev. E **83**, 041302 (2011).
[33] H. Tanaka, K. Wada, T. Suyama, and S. Okuzumi, Prog. Theor. Phys. Suppl. **195**, 101 (2012).
[34] H. Kuninaka and H. Hayakawa, Phys. Rev. E **86**, 051302 (2012).
[35] W. Harbich, *Metal Clusters at Surfaces* (Springer, Berlin, 2000).
[36] J. B. C. Pettersson and N. Marković, Chem. Phys. Lett. **201**, 421 (1993).
[37] M. Châtelet, A. D. Martino, J. Pettersson, F. Pradère, and H. Vach, Chem. Phys. Lett. **196**, 563 (1992).
[38] Y. Yamamura and T. Muramoto, Radiat. Eff. Defects Solids **130**, 225 (1994).
[39] D. J. Kenny, R. E. Palmer, C. F. Sanz-Navarro, and R. Smith, J. Phys.: Condens. Matter **14**, 185 (2002).
[40] H. P. Cheng and U. Landman, J. Phys. Chem. **98**, 3527 (1994).
[41] K. Saitoh and H. Hayakawa, Prog. Theor. Phys. **122**, 1081 (2009).
[42] S. R. Waitukaitis, H. F. Grütjen, J. R. Royer, and H. M. Jaeger, Phys. Rev. E **83**, 051302 (2011).
[43] Y. Sakiyama, S. Takagi, and Y. Matsumoto, Phys. Fluids **16**, 1620 (2004).
[44] A. Awasthi, S. C. Hendy, P. Zoontjens, S. A. Brown, and F. Natali, Phys. Rev. B **76**, 115437 (2007).
[45] L. B. Han, Q. An, S. N. Luo, and W. A. Goddard III, Mater. Lett. **64**, 2230 (2010).
[46] C. Dominik and A. G. G. M. Tielens, Astrophys. J. **480**, 647 (1997).
[47] D. J. Evans, E. G. D. Cohen, and G. P. Morriss, Phys. Rev. Lett. **71**, 2401 (1993).
[48] G. Gallavotti and E. G. D. Cohen, Phys. Rev. Lett. **74**, 2694 (1995).
[49] C. Jarzynski, Phys. Rev. Lett. **78**, 2690 (1997).
[50] P. Visco, A. Puglisi, A. Barrat, E. Trizac, and F. van Wijland, Europhys. Lett. **72**, 55 (2005).
[51] S.-H. Chong, M. Otsuki, and H. Hayakawa, Phys. Rev. E **81**, 041130 (2010).
[52] S. Joubaud, D. Lohse, and D. van der Meer, Phys. Rev. Lett. **108**, 210604 (2012).
[53] A. Naert, Europhys. Lett. **97**, 20010 (2012).
[54] H. Hayakawa and M. Otsuki, Phys. Rev. E **88**, 032117 (2013).
[55] H. Tasaki, in *Proceedings of the RIMS Workshop "Micro-Macro Duality in Quantum Analysis,"* No. 1507 (RIMS, Kyoto University, Japan, 2006), p. 102.
[56] F. Gerl and A. Zippelius, Phys. Rev. E **59**, 2361 (1999).
[57] H. Hayakawa and H. Kuninaka, Chem. Eng. Sci. **57**, 239 (2002).
[58] T. Aspelmeier, Ph.D. thesis, Georg August Universität, Göttingen, Germany, 2000.
[59] P. Valentini and T. Dumitrica, Phys. Rev. B **75**, 224106 (2007).
[60] A. E. H. Love, *A Treatise on the Mathematical Theory of Elasticity* (Dover, New York, 1906).
[61] V. I. Lebedev, USSR Comput. Math. Math. Phys. **15**, 44 (1975).
[62] A Lebedev rule of precision p can be used to correctly integrate any polynomial $f(x,y,z)$ for which the highest degree term $x^{a_x}y^{a_y}z^{a_z}$ satisfies $a_x + a_y + a_z \leqslant p$, where we adopt $p = 131$ [74].
[63] P. M. Agrawal, B. M. Rice, and D. L. Thompson, Surf. Sci. **515**, 21 (2002).
[64] J. N. Israelachvili, *Intermolecular and Surface Forces*, 3rd ed. (Academic, London, 2011).
[65] K. L. Johnson, K. Kendall, and A. D. Roberts, Proc. R. Soc. Lond. A Math. Phys. Sci. **324**, 301 (1971).
[66] H. Hertz, J. Reine Angewandte Phys. **92**, 156 (1882).
[67] L. D. Landau and E. M. Lifshitz, *Theory of Elasticity* (Pergamon, New York, 1959).
[68] D. J. Evans and D. J. Searles, Adv. Phys. **51**, 1529 (2002).
[69] H. Kuninaka and H. Hayakawa, Prog. Theor. Phys. Suppl. **178**, 157 (2009).
[70] W. Thomson, Trans. Roy. Soc. **20**, 261 (1853).
[71] W. Thomson, Phil. Mag. **5**, 4 (1878).
[72] L. D. Landau and E. M. Lifshitz, *Fluid Mechanics* (Pergamon, New York, 1959).
[73] R. Murakami, Ph.D. thesis, Kyoto University, Japan, 2014.
[74] V. I. Lebedev and D. N. Laikov, Doklady Mathematics **59**, 477 (1999).